

# TENSO: Software Package for Numerically Exact Open Quantum Dynamics Based on Efficient Tree Tensor Network Decomposition of the Hierarchical Equations of Motion

Juan C. Rodriguez Betancourt,<sup>†,§</sup> Michelle Anderson,<sup>†,§</sup> Luchang Niu,<sup>‡</sup> Xinxian Chen,<sup>†</sup> and Ignacio Franco<sup>\*,†</sup>

<sup>†</sup>*Department of Chemistry, University of Rochester, Rochester, New York 14627, United States*

<sup>‡</sup>*Department of Physics and Astronomy, University of Rochester, Rochester, New York 14627, United States*

<sup>¶</sup>*The Institute of Optics, University of Rochester, Rochester, New York 14627, United States*

<sup>§</sup>*These authors contributed equally*

E-mail: ignacio.franco@rochester.edu

March 19, 2026

## Abstract

TENSO is a versatile and powerful open-source software package for numerically exact simulations of the dynamics of quantum systems immersed in structured thermal environments. It is based on a tree tensor network decomposition of the hierarchical equations of motion (HEOM) that efficiently curbs its curse of dimensionality with bath complexity. As such, TENSO enables exact non-Markovian open quantum dynamics simulations even with complex environments typical of chemistry and quantum information science. TENSO allows for time-dependent drive in the system, and for non-commuting fluctuations. More generally, TENSO efficiently propagates the dynamics for any method with a generator of the dynamics that can be expressed in a sum-of-products form, including the HEOM and multi-layer multiconfigurational time-dependent Hartree methods. TENSO enables simulations using tensor

trees and trains of arbitrary order, and implements three propagation strategies for the coupled master equations; two fixed-rank methods that require a constant memory footprint during the dynamics and one adaptive rank method with a variable memory footprint controlled by the target level of computational error. In contrast to the accompanying theory and algorithmic paper [J. Chem. Phys. **163**, 104109 (2025)] the focus here is on the practical usage and applications of TENSO with underlying theoretical concepts introduced only as needed.

## 1 Introduction

Open quantum systems refer to systems interacting with their quantum environment. This interaction introduces quantum noise or decoherence and is responsible for ubiquitous processes in nature such as dephasing, energy relaxation and the thermalization of quantum systems making a detailed understanding of open quantum dynamics essential in chemistry, physics, and quantum information science.<sup>1-7</sup>

Further, elucidating decoherence mechanisms is necessary to engineer quantum environments for quantum and chemical control tasks.<sup>8–13</sup> The aim of TENS0, Tensor Equations for Non-Markovian Structured Open Systems,<sup>14,15</sup> is to predict the dynamics of quantum systems interacting with macroscopic thermal environments of arbitrary complexity using the numerically exact hierarchical equations of motion (HEOM).<sup>16</sup> TENS0 combines the hexcitonic generalization of the HEOM<sup>17</sup> –which unites HEOM variants and exposes their mathematical structure– with a tree tensor network (TTN) decomposition which enables numerically efficient simulation.

In open quantum dynamics it is customary to decompose the Hamiltonian,  $H = H_S + H_{SB} + H_B$ , of the quantum universe into Hamiltonians of a system  $H_S$ , a bath  $H_B$  and their interaction  $H_{SB}$ .<sup>1</sup> Since the bath is usually macroscopic, the strategy in open quantum dynamics is to develop quantum master equations (QMEs) that capture its influence on the system without propagating the bath degrees of freedom explicitly. A variety of approaches have been developed to simulate open quantum system dynamics.<sup>1,6,7,18–22</sup> Of particular interest are numerically exact QMEs as they can be used to model a large class of problems of importance in chemistry and quantum information science with an accuracy that can be assured. This contrasts with common strategies based on the Born-Markov approximation that only apply to systems weakly coupled to fast environments with short memory time,<sup>1</sup> conditions that are often too restrictive for chemical dynamics.

The HEOM is a powerful method for numerically exact open quantum dynamics for systems embedded in thermal Bosonic environments.<sup>16,17,23–25</sup> In the case of linear system-bath coupling, the bath correlation function (BCF) contains all information about the bath needed to construct the quantum master equation. To make the QME numerically tractable, HEOM decomposes the BCF into a series of  $K$  complex decaying exponentials which allows the influence of the environment to be captured by a hierarchy of auxiliary density matrices

(ADMs). In the limit of an infinitely large hierarchy the simulation is exact, but in practice the hierarchy must be truncated at a level which maintains accuracy and controls computational expense. HEOM has been employed effectively for models of spectroscopy, and for charge and energy transport in photosynthetic complexes, molecular aggregates, Holstein models, and organic photovoltaic cells.<sup>26–32</sup> The main challenge of HEOM is that the cost of the quantum dynamics grows exponentially with the number of features  $K$  in the bath, thus limiting the use of HEOM to simple model problems with unstructured environments.

Due to its importance, several computational packages implement HEOM simulations, including QUTIP, PYHEOM, HIERARCHICALEOM.JL, GPU-HEOM, and DM-HEOM.<sup>23,27,33–35</sup> However, these implementations are often limited by the number of features  $K$  that can be included, and present-day capabilities are insufficient to capture chemically realistic environments, especially when low temperature correction terms are required.

To mitigate this curse of dimensionality, recently we introduced a TTN decomposition of the HEOM (TTN-HEOM) which allows for efficient compression of the simulation space thus enabling simulations of open quantum systems interacting with environments with large numbers of features.<sup>14</sup> Our approach further allows for time-dependent system Hamiltonians and multiple baths, providing a useful and versatile method to investigate dissipative dynamics.

Tensor network decompositions represent the state of the art in the simulation of many-body systems.<sup>36–43</sup> In particular, they are the basis for the powerful multi-layer multi-configurational time-dependent Hartree (ML-MCTDH)<sup>37,44,45</sup> method which is the gold standard in high-dimensional closed quantum dynamics simulations. Our TTN-HEOM developments are parallel to the ML-MCTDH as the three main principles (sum of product dynamical generator, TTN decomposition, and Dirac-Frenkel time-dependent variational principle (TDVP)<sup>44,46–48</sup> to isolate the equations of motion) are identical. However, while ML-MCTDH is designed for unitary dynamics, the

TTN-HEOM is designed for thermal dissipative dynamics.

In particular, `TENSO` arranges the large set of ADMs in the HEOM formalism into an extended density operator (EDO). This higher order EDO is decomposed into core tensors using the TTN representation. To optimally evolve the TTN such that it correctly represents the EDO, `TENSO` applies the TDVP to develop QMEs for the core tensors. The `TENSO` implementation of this QME provides efficient, stable, error-controlled evolution best suited for open quantum dynamics with strong coupling and complicated bath spectral density structure.

We illustrate the usage of `TENSO` and demonstrate its versatility and wide-applicability to open quantum dynamics through three examples. First is the quintessential spin-boson problem which is a key model in spectroscopy and quantum information.<sup>19,49,50</sup> Using this model, we will illustrate the fundamental features of `TENSO`, how to perform simulations with structured spectral densities, how `TENSO` easily addresses non-commuting fluctuations, how to invoke time-dependent Hamiltonians, and how to manipulate the convergence. We will also briefly mention `TENSO`'s extension to MCTDH, emphasizing the adaptability of `TENSO`'s underlying structure to other master equations with propagators in sum of products form. We then address the Fenna-Matthews-Olson (FMO)<sup>51,52</sup> complex, a paradigmatic multilevel model problem in the study of photosynthetic energy capture.<sup>53-58</sup> We use it to demonstrate how to employ `TENSO` to address multilevel systems coupled to multiple structured baths. Our third example is the sudden death of entanglement between two qubits interacting with a thermal environment.<sup>59</sup> We use it to demonstrate how `TENSO` can address problems in quantum information.

The structure of this paper is as follows. Section 2 reviews the hexcitonic HEOM and its TTN decomposition. Section 3.1 demonstrates the installation, usage and capabilities of `TENSO` through representative numerical examples. Section 4 provides information on the architecture and design of the `TENSO` package,

and section 5 discusses modifications which can be made to the `TENSO` code to address specialized applications.

## 2 Methods

We now provide an overview of the most important theory underlying `TENSO`. Refs. 17 and 14 provide detailed derivations, and a full discussion of the propagation strategies employed.

### 2.1 Bath Correlation Function and its Decomposition into Features

The HEOM focuses on the open quantum dynamics of systems immersed into an environment that can be described as a collection of harmonic oscillators with Hamiltonian

$$H_B = \sum_j \left( \frac{p_j^2}{2m_j} + \frac{m_j \omega_j^2 x_j^2}{2} \right). \quad (1)$$

Here,  $x_j$  and  $p_j$  are the position and momentum of the  $j$ -th oscillator with frequency  $\omega_j$  and effective mass  $m_j$ . The system-bath coupling Hamiltonian is of the form  $H_{SB} = Q_S \otimes X_B$  where  $Q_S$  is a system operator and  $X_B = \sum_j c_j x_j$  is a collective bath coordinate. Here,  $c_j$  quantifies the coupling strength between the system operator and the  $j$ th bath mode. Harmonic models of the environment are broadly used as any environment can be represented by this model up to second order in perturbation theory.<sup>60,61</sup> Further, this is commonly applicable in the thermodynamic limit as the system-bath interaction is diluted over a macroscopic number of modes.<sup>62,63</sup> For harmonic environments, the dynamical properties of the bath are completely captured by the BCF,  $C(t) = \langle \tilde{X}_B(t) \tilde{X}_B(0) \rangle$ , where  $\tilde{X}_B(t)$  is the collective bath coordinate in the interaction picture of  $H_S + H_B$  and the expectation value is over the bath thermal state.<sup>19</sup> Formally the

BCF can be expressed as

$$C(t) = \int_{-\infty}^{+\infty} \mathcal{J}(\omega) f_{\text{BE}}(\beta\omega) e^{-i\omega t} d\omega, \quad (2)$$

where

$$\mathcal{J}(\omega) = \frac{\sum_j |c_j|^2 [\delta(\omega - \omega_j) - \delta(\omega + \omega_j)]}{(2m_j\omega_j)} \quad (3)$$

is an odd extension of the bath spectral density, a quantity that summarizes the frequencies  $\{\omega_j\}$  of the oscillators in the bath and specifies their coupling strengths to the system. The function  $f_{\text{BE}}(\beta\omega) = (1 - e^{-\beta\omega})^{-1}$  is related to the Bose–Einstein distribution and  $\beta = 1/k_B T$  the inverse temperature. Without loss of generality, the residue theorem is used to decompose the BCF into a sum of complex exponential functions referred to as features, typically via Padé<sup>64</sup> or Matsubara<sup>65</sup> expansions. This allows us to write the BCF as

$$C(t) = -2\pi i \sum_i \text{Res}_{z=\zeta_i} [\mathcal{J}(z)] f_{\text{BE}}(\beta\zeta_i) e^{-i\zeta_i t} - 2\pi i \sum_j \text{Res}_{z=\xi_j} [f_{\text{BE}}(z)] \mathcal{J}(\xi_j/\beta) e^{-i(\xi_j/\beta)t}, \quad (4)$$

where  $\{\zeta_i\}$  are the first-order poles in the lower half of the complex plane of  $\mathcal{J}(\omega)$  and  $\{\xi_i\}$  are those of  $f_{\text{BE}}(\beta\omega)$ . By this method, the BCF can always be decomposed in terms of complex decaying exponentials such that  $C(t) = \sum_{k=1}^K c_k e^{\gamma_k t}$  and  $C^*(t) = \sum_{k=1}^K \bar{c}_k e^{\gamma_k^* t}$  where  $c_k, \bar{c}_k$  and  $\gamma_k$  are complex numbers. Each term  $k$  in Eq. (4) corresponds to a feature and  $K$  is the total number of features.<sup>17</sup> The first set of features arise due to the spectral density itself, while the second set arise due to the thermal factor and is referred to as low temperature corrections.

Two common models for the spectral density are the Drude-Lorentz (DL) model and the Brownian oscillator (BO) model.<sup>19,50</sup> The DL spectral density,

$$J_{\text{DL}}(\omega) = \frac{2\lambda}{\pi} \frac{\omega_c \omega}{\omega^2 + \omega_c^2} \quad (5)$$

describes an Ohmic environment with  $\lambda$  reorganization energy and  $\omega_c$  cut-off frequency. Drude-Lorentz environments contribute to a single, simple decaying exponential with characteristic relaxation timescale of  $\omega_c^{-1}$ . In turn, the BO spectral density is expressed as

$$J_{\text{BO}}(\omega) = \frac{4\lambda}{\pi} \frac{\eta\omega_0^2\omega}{(\omega^2 - \omega_0^2)^2 + 4\eta^2\omega^2}, \quad (6)$$

and describes the contribution of a discrete harmonic oscillator where  $\lambda$  is its reorganization energy,  $\omega_0$  its natural frequency and  $1/\eta$  its damping rate. Brownian oscillators contribute two oscillatory-decaying features to the BCF decomposition. In TENS0, the actual spectral density used for the BO oscillator is

$$J_{\text{BO}}(\omega) = \frac{4\lambda\eta}{\pi} \frac{(\omega_0'^2 + \eta^2)\omega}{[(\omega + \omega_0')^2 + \eta^2][(\omega - \omega_0')^2 + \eta^2]} \quad (7)$$

which is mathematically equivalent to the standard Brownian oscillator in Eq.(6) under the parameter mapping  $\omega_0' = \sqrt{\omega_0^2 - \eta^2}$ , which corresponds to the effective frequency under damping ( $\eta < \omega_0$ ). The factored form is used because its relevant poles are simply located at  $\pm\omega_0' - i\eta$ , which makes the decomposition in Eq. (4) straightforward.

In chemical dynamics it is often possible to define a spectral density as a combination of DL and BO terms as<sup>10</sup>

$$J(\omega) = J_{\text{DL}}(\omega) + \sum_b J_{\text{BO}}^{(b)}(\omega). \quad (8)$$

Environments with a large number of features,  $K$ , are referred to as highly structured. Since the numerical cost of the open quantum dynamics scales exponentially with  $K$ , the computations become increasingly challenging. In fact, HEOM calculations using standard methods are only feasible with one to five features.

## 2.2 Hierarchical Equations of Motion

While the full dynamics of the composite system with density matrix  $\rho(t)$  is unitary, the dy-

namics of the reduced system,

$$\rho_S = \text{Tr}_B(\rho(t)) \quad (9)$$

is non-unitary, where  $\text{Tr}_B$  indicates a trace over the bath degrees of freedom. The dynamical map of  $\rho_S(t)$  is,<sup>66</sup>

$$\tilde{\rho}_S(t) = \mathcal{T}\tilde{\mathcal{F}}(t,0)\rho_S(0) \quad (10)$$

with time-ordering operator  $\mathcal{T}$  and

$$\tilde{\mathcal{F}}(t,0) = e^{-\int_0^t ds \tilde{Q}_S^\times(s) \int_0^s du (C(s-u)\tilde{Q}_S(u))^\times}. \quad (11)$$

Throughout, the tilde indicates operators in the interaction picture of  $H_0(t) = H_S(t) + H_B$ ,

$$\tilde{O}(t) = (\mathcal{T}e^{-i\int_0^t H_0(t')dt'})^\dagger O(t) (\mathcal{T}e^{-i\int_0^t H_0(t')dt'}). \quad (12)$$

For any operator  $A$  we use the convention  $A^\times B = A^>B - A^<B = AB - BA^\dagger$ .

Employing the decomposition of the structured bath into features following Eq. (4) and calculating the time-derivatives in the formal evolution of  $\tilde{\rho}_S(t)$  reveals that the influence of the thermal environment is exactly captured by an infinite hierarchy of auxiliary density matrices, ADMs,  $\{\varrho_{\vec{n}}(t)\}$ , of the same dimension,  $M \times M$ , as the system density matrix. Here  $\vec{n} = (n_1, \dots, n_k, \dots, n_K)$  is a  $K$  dimensional index, with  $K$  being the number of features of the bath. Each  $n_k$  runs formally from 0 to infinity and practically from 0 to a truncation limit known as the hierarchy depth.

TENSO takes the generalized bexcitonic view of HEOM<sup>17</sup> where the system is conceptualized as interacting with a collection of fictitious, bosonic quasiparticles called bexcitons, each corresponding to a bath feature. In the bexcitonic HEOM, the ADMs are arranged into an extended density operator (EDO). The EDO is  $|\Omega(t)\rangle = \sum_{\vec{n}} \varrho_{\vec{n}}(t)|\vec{n}\rangle$  which is specified in the basis given by  $|\vec{n}\rangle = |n_1\rangle \otimes \dots \otimes |n_k\rangle \otimes \dots \otimes |n_K\rangle$  such that a given ADM is found as  $\varrho_{\vec{n}}(t) = \langle \vec{n} | \Omega(t) \rangle$ . The system density matrix is  $\rho_S(t) = \varrho_{\vec{0}}(t) = \langle \vec{0} | \Omega(t) \rangle$ , meaning it is found where all indices in  $|\vec{n}\rangle$  are zero.

The equation of motion of the EDO is given by,<sup>14,17</sup>

$$\frac{d}{dt} |\Omega(t)\rangle = \left( -iH_S^\times(t) + \sum_{k=1}^K \mathcal{D}_k \right) |\Omega(t)\rangle, \quad (13)$$

where  $\mathcal{D}_k$  is the dissipator associated with the  $k$ -th bath feature, or bexciton. In particular, for each  $k$ ,

$$\mathcal{D}_k = \gamma_k \hat{\alpha}_k^\dagger \hat{\alpha}_k + (c_k Q_S^> - \bar{c}_k Q_S^<) \hat{z}_k^{-1} \hat{\alpha}_k^\dagger - Q_S^\times \hat{\alpha}_k \hat{z}_k \quad (14)$$

with  $\hat{z}_k$ , the metric, being any invertible operator which commutes with  $\hat{\alpha}_k^\dagger \hat{\alpha}_k$ ,  $\hat{\alpha}_k^\dagger$  and  $\hat{\alpha}_k$  are the bosonic creation and annihilation operators for the  $k$ th bexciton,  $([\hat{\alpha}_k, \hat{\alpha}_{k'}^\dagger]) = \delta_{k,k'}$ . In the bexcitonic view of HEOM, each feature,  $k$ , is associated with a fictitious, bosonic quasiparticle. The operator  $\hat{\alpha}_k^\dagger$  creates a  $k$ th bexciton and the operator  $\hat{\alpha}_k$  destroys it. With  $|\vec{n}\rangle$  we associate a state with  $|n_k\rangle$  bexcitons created for each  $k$ . The  $K$  bexcitons constitute a coarse grained, but numerically exact, representation of the macroscopic bath but are not physical particles associated with modes of the bath. Although useful for monitoring convergence of the dynamics, bexcitons do not provide physical information about the bath state.

For each feature  $k$ , the bexcitonic ladder must be truncated at a maximum occupation  $(N_k - 1)$ , the depth of the  $k$ th-bexciton, to allow for practical simulations.<sup>17</sup> For an  $M$ -state system coupled to  $K$  bath modes, each truncated at  $N_k = \mathcal{O}(N)$ , the memory cost of the EDO scales as  $\mathcal{O}(M^2 N^K)$ . This exponential growth of memory requirements with  $K$  constitutes the principal limitation of HEOM simulations.<sup>14</sup> This problem is especially severe for highly structured spectral densities and at low temperatures where many features are required.

Equation (13) specifies a class of QMEs. Conventional HEOM uses  $\hat{z}_k = i(\hat{\alpha}_k^\dagger \hat{\alpha}_k)^{-1/2}$  and a number basis representation of  $|\vec{n}\rangle$ . By adjustment of the metric and basis representation of  $|\vec{n}\rangle$ , we can recover and develop many variants of HEOM.<sup>17</sup>

## 2.3 Tree Tensor Network Decomposition

The curse of dimensionality in HEOM can be mitigated by recognizing that the EDO contains significant redundancy that can be systematically compressed via tensor network representations, greatly reducing memory requirements.<sup>14,67–69</sup> We begin by reexpressing the EDO. Analogously to the density matrix of the system,  $\rho_S(t)$ , with matrix elements  $[\rho_S]_{ij} = \langle i | \rho_S(t) | j \rangle$  in a basis  $\{|i\rangle\}$  spanning the system Hilbert space, the EDO can be represented as

$$[\Omega(t)]_{ijn_1 \dots n_K} = \langle i | \langle n_1 \dots n_K | \Omega(t) | j \rangle, \quad (15)$$

where  $\{|n_k\rangle\}_{n_k=0}^{N_k-1}$  is the truncated number basis for the  $k$ th-bexciton. The dynamics of  $\Omega(t)$  in Eq. (13) can be written compactly as<sup>14</sup>

$$\frac{d}{dt} \Omega(t) = \mathcal{L}(t) \Omega(t), \quad (16)$$

where  $\mathcal{L}(t)$  is the tensor representation of the Liouvillian superoperator generating the dynamics in Eq. (13). Because the basis factorizes as  $|i\rangle \otimes |j\rangle \otimes |n_1\rangle \otimes \dots \otimes |n_K\rangle$ ,  $\mathcal{L}(t)$  admits the operator in sum of products (SoPs) form,

$$\mathcal{L}(t) \equiv \sum_{m=1}^{5K+2} h_m^>(t) \otimes h_m^<(t) \otimes h_m^{(1)} \otimes \dots \otimes h_m^{(K)} \quad (17)$$

with local operators  $h_m^{(\kappa)}$  where the index  $m$  runs over all terms in Eq. (13) and ( $\kappa = >, <, 1, \dots, K$ ). Each dissipator  $\mathcal{D}_k$  contributes five terms and the unitary Liouvillian,  $-iH_S^\times(t)$ , contributes two. Here  $h_m^>(t)$  and  $h_m^<(t)$  act on the system space while  $h_m^{(k)}$  acts on the truncated  $k$ th-bexciton space.

The EDO is a high dimensional tensor. The memory requirements to describe a tensor are exponential in the tensors order, meaning that for a tensor  $A_{a_1 \dots a_D}$ , where the  $a_i = 1, \dots, R$ , the tensor requires  $O(R^D)$  memory space. Performing mathematical operations on the tensor which require access to all elements thus also scales catastrophically. To avoid this, the EDO is compressed by expressing it as a network of low-order core tensors. The tree is assembled

in general by repeated applications of the singular value decomposition<sup>70</sup> (SVD), a procedure known as the hierarchical Tucker decomposition (HTD).<sup>71,72</sup> When performing the decomposition, small singular values judged to be relatively unimportant can be discarded, with the number of retained singular values known as the rank of the bond,  $R$ . Contractions are performed between the network's core tensors according to the topology of a tree graph and the lowest order tensors possible are employed for efficiency. The lowest order that allows for the assembly of an arbitrary size TTN is three. The decomposition will always include  $K$  order three core tensors with  $K - 1$  contractions.

The simplest TTN topology is a tensor train (TT),

$$\begin{aligned} \Omega_{ijn_1 \dots n_K} = & \\ & \sum_{a_1 a_2 \dots a_{K-1}}^{R_1 R_2 \dots R_{K-1}} A_{ij a_1}^{(0)} U_{a_1 n_1 a_2}^{(1)} U_{a_2 n_2 a_3}^{(2)} \dots U_{a_{K-1} n_{K-1} n_K}^{(K-1)} \end{aligned} \quad (18)$$

where  $\{a_s\}_{s=1}^{K-1}$  are bond indices of ranks  $\{R_s\}$ . Similarly, a general TTN is written as,

$$\begin{aligned} [\Omega(t)]_{ijn_1 \dots n_K} = & \\ & \sum_{a_1 \dots a_{K-1}}^{R_1 \dots R_{K-1}} A_{ij a_1}^{(0)} U_{a_1 \beta_1 \gamma_1}^{(1)} \dots U_{a_{K-1} \beta_{K-1} \gamma_{K-1}}^{(K-1)} \\ & \equiv [\text{Con}(A^{(0)}(t), U^{(1)}(t), \dots, U^{(K-1)}(t))]_{ijn_1 \dots n_K} \end{aligned} \quad (19)$$

where  $\text{Con}(\cdot)$  denotes contraction of the TTN core tensors,  $A^{(0)}(t), U^{(1)}(t), \dots, U^{(K-1)}(t)$ , according to the chosen network topology, and each pair  $(\beta_s, \gamma_s)$  corresponds either to a bath index  $n_k$  (open bond) or to a virtual bond  $a_u$  (internal contraction).

The semi-unitary core tensors  $U^{(s)}(t)$  in the TTN are chosen to satisfy

$$\sum_{\beta\gamma} [U^{(s)}(t)]_{a'_s, \beta\gamma}^* [U^{(s)}(t)]_{a_s, \beta\gamma} = \delta_{a'_s a_s}, \quad (20)$$

but the root tensor  $A^{(0)}(t)$  is not constrained to be semi-unitary. Following standard practice, the system indices  $(i, j)$  and the first bond  $a_1$  are placed in the root tensor so that the physical system degrees of freedom remain uncom-

pressed while the bath degrees of freedom are compacted.

For a hierarchy of depth  $N$  and TTN bond ranks  $R_s = \mathcal{O}(R)$ , the TTN storage scales as

$$\mathcal{O}(M^2R + KNR(N + R)), \quad (21)$$

thereby eliminating the exponential dependence on  $K$  and providing a controllable, systematically improvable approximation that becomes exact as the ranks increase. The equation of motion for the tensor network is determined by the TDVP applied using the Liouillian Eq. (16). The derivation is detailed in previous work.<sup>14</sup>

The most important result is the determination of equations of motion for the root and core tensors, admitting general numerical methods for solving coupled differential equations, for any master equation which admits a sum of products form for  $\mathcal{L}(t)$ . This allows flexibility in the implementation of propagation methods, including both fixed rank and adaptive rank integration schemes.

## 3 Numerical examples

### 3.1 Obtaining and Installing TENS0

TENS0 is a python package which can be obtained from github: <https://github.com/ifgroup/pytenso>. Users must have python 3.13 or later installed to run TENS0. TENS0 further relies on the packages `numpy`,<sup>73</sup> `scipy`,<sup>74</sup> `pytorch`,<sup>75</sup> `torchdiffeq`<sup>76</sup> and `tqdm`.<sup>77</sup> These packages provide high-level interfaces designed to simplify tensor operations across diverse computational platforms, including various CPU and GPU architectures. For this tutorial, users should also have `matplotlib`<sup>78</sup> available. A python virtual environment should be prepared for TENS0 and these packages made available in it prior to installation. A thorough guide to preparing virtual environments and installing python packages for Windows, Macintosh, and Linux users can be found in the official Python 3 documentation. Package managers Anaconda and Pip can also be used.

Once the environment has been prepared and TENS0 installed, run it as `python <input file>`. TENS0 reads all parameters of the system and bath from the input file using energy units of  $\text{cm}^{-1}$ , time units of fs, and temperature units of K.

### 3.2 Overview

In this section we will use three sample systems, the spin-boson, the FMO complex, and a pair of qubits, all selected due to their important roles in quantum dynamics, to demonstrate how to employ TENS0 on research problems ranging from energy transport to entanglement dynamics.

All examples in this tutorial should run on a laptop or desktop computer with the exception of the Fenna-Matthews-Olson complex example which will require a cluster to run in its entirety, especially with the more complicated spectral density. TENS0 excels at and provides the largest performance gains when handling difficult problems for HEOM, those which have complicated spectral densities which cannot be represented by a single Drude-Lorentz or Brownian bath alone, or those which need large hierarchy depths.

### 3.3 Example 1: Spin-Boson

The spin-boson model, a single two level system interacting with a thermal boson bath,<sup>19,49</sup> has been used to test the performance of quantum simulation methods, Markovian and non-Markovian,<sup>79-82</sup> to study the impacts of bath parameters in open systems,<sup>83,84</sup> and to understand physical processes involving two-level systems (TLS), ranging from spontaneous emission<sup>49,85</sup> to superconducting qubit relaxation.<sup>86,87</sup> It remains an important system of study.

The spin-boson system Hamiltonian is given by

$$H_S = \frac{\Delta\epsilon}{2}\sigma_z + V\sigma_x, \quad (22)$$

with energy gap  $\Delta\epsilon$ , tunneling amplitude  $V$ , and Pauli operators  $\sigma_z$  and  $\sigma_x$ . The system-

bath coupling is

$$H_{\text{SB}} = \frac{\sigma_z}{2} \otimes X_{\text{B}}. \quad (23)$$

We will use the spin-boson problem to demonstrate the basic usage of TENS0, how to specify the spectral density of a structured bath, how to invoke a time-dependent Hamiltonian, and how to understand parameters that may impact numerical convergence of the results.

### 3.3.1 Dynamics in a structured bath

Listing 1, shows a complete TENS0 input file specifying an HEOM calculation for a spin in interaction with a bath whose spectral density includes a DL and a BO term. The file is broken into three sections, (1) importing modules (2) bath correlation function definition and (3) propagation. All HEOM examples in this tutorial will require the same import statements. Simulation parameters used in Listing 1 are given in Table 1.

In TENS0 the `gen_bcf` helper function builds the BCF. It takes the cutoff frequencies, the reorganization energies, widths, and the resonant frequencies as lists that encode the spectral densities' structures. To label the two types of SDs, TENS0 uses the suffixes `_d` and `_b` for the DL and Brownian SD, respectively. To use the Matsubara decomposition scheme, the argument `'Pade'` is replaced with `'Matsubara'` in the call to `gen_bcf`. It is also possible to implement custom BCFS's and their decompositions, as detailed in section 5.

Propagation in TENS0 is performed with the `system_multibath` function. This helper function can address one or more baths. It takes all system information, the BCF or BCF's in list form, system-bath coupling operators, and all additional simulation parameters such as integrator tolerances or the tensor network decomposition scheme.

```

1 # Import statements for simulation
2 from math import ceil
3 import os
4 import json as json
5 import numpy as np
6 from tqdm import tqdm
7 from tenso.prototypes.bath import gen_bcf

```

Table 1: **Simulation parameters for the spin–boson model.** The system parameters include the energy bias  $\Delta\epsilon$  and the tunneling coupling  $V$ . The bath spectral density is modeled as a sum of Drude–Lorentz (DL) and Brownian oscillator (BO) contributions, parameterized by the reorganization energy  $\lambda$ , the cutoff frequency  $\omega_c$ , the damping coefficient  $\eta$ , and the vibrational frequency  $\omega'_0$ . The resulting spectral density is shown in Fig. 1(b). All parameters are given in  $\text{cm}^{-1}$ .

Parameter	Value ( $\text{cm}^{-1}$ )
$\Delta\epsilon$	1500
$V$	300
$\lambda, \omega_c$ (DL)	540, 70
$\lambda, \eta, \omega'_0$ (BO)	161.6, 10, 1243

```

8 from tenso.prototypes.heom import
   system_multibath
9 # Import statement required to plot
   results
10 import matplotlib.pyplot as plt
11
12 # Generate the decomposed bath
   correlation function
13 # for HEOM propagation
14 bath_simulation = gen_bcf(
15     re_d=[540], # Drude-Lorentz
   Reorganization energy (cm^{-1})
16     width_d=[70], # Drude-Lorentz spectral
   density cut-off frequency (cm
   ^{-1})
17     freq_b=[1243], # Brownian spectral
   density frequency (cm^{-1})
18     re_b=[161.6], # Brownian spectral
   reorganization energy (cm^{-1})
19     width_b=[10], # Brownian spectral
   width (cm^{-1})
20     temperature=300, # Temperature of this
   bath
21     decomposition_method='Pade',
22     n_ltc=1,) # Low temperature correction
   terms
23 end_time = 1000 # Propagation time in fs
24 dt = 1 # Time step size in fs
25 wfn = np.array([0.0, 1.0], dtype=np.
   complex128) # Initial wavefunction
26 out="tutorial_1" # Base name for the
   output
27
28 # Generate the propagator to evolve the
   system density matrix
29 propagator = system_multibath(

```

```

30  fname=out, # Specify output file
31  init_rdo=np.outer(wfn, wfn.conj()), #
    Set system initial condition
32  sys_ham=np.array
    ([[ -750.0, 300.0], [300.0, 750.0]],
    dtype=np.complex128), # Set the
    system Hamiltonian (cm-1)
33  sys_ops=[np.array([[ -0.5, 0.0],
    [0.0, 0.5]], dtype=np.complex128)],
    # Set the H{SB} system-bath
    coupling operator(s)
34  bath_correlations=[bath_simulation], #
    Specify bath correlation function
    (s) generated by gen_bcf
35  dim=25, # Hierarchy depth
36  end_time=end_time, # End time of the
    simulation
37  step_time=dt,) # Time step size
38  # Perform the dynamics simulation and
    generate a progress bar
39  progress_bar = tqdm(propagator,total=ceil
    (end_time/dt))
40  for _t in progress_bar:
41  progress_bar.set_description(f'@{_t:
    .2f} fs')
42
43  # Load results from the output file into
    a local array
44  results = np.loadtxt(out+".dat.log",dtype
    =np.complex128)
45  # Plot the populations of the two state
    of the spin-boson
46  plt.plot(np.real(results[:,0]),np.real(
    results[:,1]),np.real(results[:,0]),np
    .real(results[:,4]))
47  plt.xlabel("Time (fs)")
48  plt.ylabel("Population")
49  plt.savefig(out+'.png')
50  plt.show()

```

Listing 1: **Dynamics of a Structured Bath Spin-Boson model:** Complete input file for running a spin-boson propagation with a structured bath.

On completion, this calculation will display a figure of the populations of the two states and save the image to a file. The output file, tutorial.1.dat.log will record the complex values of all entries in the density matrix of the evolving system and output them in the order  $\rho_{1,1}$   $\rho_{1,2}$ ...  $\rho_{n,n-1}$ ,  $\rho_{n,n}$  for each simulation time step. The dynamics are shown in Fig. 1.

### 3.3.2 Comparison of Different Tensor Decompositions

TENSO incorporates two built-in TTN decomposition schemes, the Tensor-Train (TT) decomposition and the balanced tensor tree (BTT) decomposition. The binary BTT is the default option and will be appropriate for most uses. The first example in Listing 1 addressed a spin-boson system using the BTT. We now demonstrate that a TT decomposition produces equivalent results. To produce an equivalent calculation with a TT decomposition, we add the line `frame_method= 'train'`, in Listing 1 as an extra argument to `system_multibath`. This is the only needed modification.

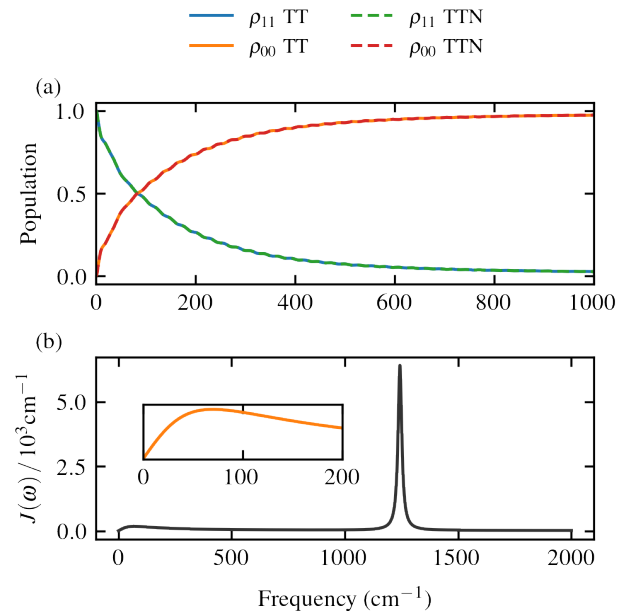


Figure 1: **Structured Spin-Boson Quantum Dynamics.** (a) Population relaxation dynamics of the spin-boson system, with the excited state in blue and ground state in orange, showing that dynamics are identical whether the TT or BTT tensor network decomposition is employed. (b) Structured spectral density employed in the simulation.

Fig. 1 shows results of both the TT and BTT simulations of the spin-boson problem, demonstrating that they produce equivalent results. The dynamics show decay of the population and small oscillations attributed to interaction with the underdamped Brownian mode whose

presence is very notable in the spectral density, Fig. 1(b). Note that all of TENS0’s convergence parameters controlling accuracy and expense, which will be discussed in depth in section 3.3.6, are identical for these calculations. In this particular case, the convergence and performance of the simulation is not significantly impacted by the chosen tensor configuration.

### 3.3.3 Non-Commuting Fluctuations

TENS0 enables the modeling of open quantum systems coupled to non-commuting fluctuations. In this situation, an open quantum system is coupled to two or more distinct, independent thermal baths. Specifically, with the superscript  $b$  referencing distinct baths,  $H_{SB} = \sum_b Q_S^{(b)} \otimes X_B^{(b)}$ ,  $H_B = \sum_{j,b} \left( \frac{(p_j^{(b)})^2}{2m_j^{(b)}} + \frac{m_j^{(b)}(\omega_j^{(b)})^2(x_j^{(b)})^2}{2} \right)$ , and the  $Q_S^{(b)}$  do not commute. These systems may display interesting phenomena, including the apparent suppression of spin relaxation by decoherence<sup>88,89</sup> but their treatment can be challenging.<sup>88–91</sup> As many systems relevant to quantum information science involve non-commuting fluctuations, including system interacting simultaneously with radiation and phonon fields, addressing them is an important capability of TENS0.

A simple example of a system coupled to non-commuting fluctuations is a spin-boson problem where  $H_{SB} = \frac{1}{2}\sigma_x \otimes X_B^{(1)} + \frac{1}{2}\sigma_z \otimes X_B^{(2)}$ . We calculate dynamics of the system specified in Listing 1 and in Table 1 with addition of a second, identical bath with  $Q_S^{(2)} = \frac{1}{2}\sigma_x$ . This requires changing the propagator as shown in Listing 2.

```

1 # Set up the two system-bath coupling
  operators
2 bath_op1 = np.array
  ( [[-0.5,0.0],[0.0,0.5]], dtype=np.
  complex128)
3 bath_op2 = np.array
  ( [[0.0,0.5],[0.5,0.0]], dtype=np.
  complex128)
4
5 propagator = system_multibath(
6   fname=out,
7   init_rdo=np.outer(wfn, wfn.conj()),
8   sys_ham=np.array
  ( [[-750.0,300.0],[300.0,750.0]],

```

```

dtype=np.complex128),
9   sys_ops=[bath_op1,bath_op2], # Set the
  H_{SB} system-bath coupling
  operators
10  bath_correlations=[bath_simulation,
  bath_simulation], # Specify two
  identical correlation functions
11  dim=30,
12  end_time=end_time,
13  step_time=dt,)

```

Listing 2: **Non-Commuting Fluctuations:** Code modifications needed to set up a propagator when the system is coupled to two baths by non-commuting operators.

The dynamics of the system coupled to the two non-commuting fluctuations, shown in Fig. 2, differ significantly from those of the system coupled to a single bath in Fig. 1. The total reorganization energy has doubled with the inclusion of the second bath, leading to faster relaxation. The apparent slowing of relaxation at approximately 50 fs appears due to the competing influences of the two baths interacting with the system.

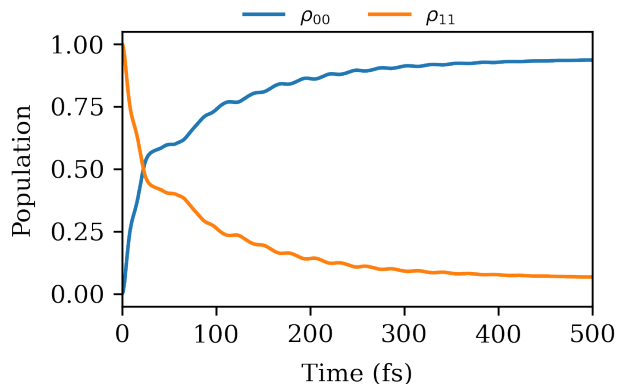


Figure 2: **Spin-Boson With Two Baths:** Evolution of a spin-boson system, coupled to two non-commuting fluctuations.

### 3.3.4 Driven Structured Spin-Boson Model

TENS0 supports time-dependent Hamiltonians, enabling the simulation of driven phenomena in the presence of decoherence, such as photoexcitation of molecules in the condensed phase, spectroscopy, quantum control and quantum information processing.

Here, we simulate a spin-boson model resonantly driven by a  $\frac{\pi}{2}$ -pulse. In the absence of decoherence, this control pulse implements a perfect Hadamard gate on this qubit, transitioning it from the ground state  $|0\rangle$  to  $\frac{1}{\sqrt{2}}(|0\rangle + |1\rangle)$ . The total system Hamiltonian is given by

$$H_S = \sigma_z \frac{\Delta\epsilon}{2} - \sigma_x \mu_0 E(t) \quad (24)$$

where  $\mu_0$  is the transition dipole moment and  $E(t)$  is the time-dependent laser field. The driving is realized by a single  $\pi/2$ -area Gaussian laser pulse, determined from the area theorem,<sup>92</sup>

$$E(t) = E_0 \exp\left[-\frac{1}{2}\left(\frac{t-\tau}{\sigma}\right)^2\right] \cos(\omega_L t), \quad (25)$$

where  $E_0$  is the peak electric field amplitude,  $\omega_L$  is the driving frequency, and  $\sigma$  is related to the pulse full width at half maximum (FWHM) by  $\sigma = \text{FWHM} / (2\sqrt{2\ln 2})$ . In our simulations, FWHM corresponds to a value of 2.1233045 fs. The system-bath coupling corresponds to pure dephasing noise, which is appropriate in many quantum computing investigations where dephasing is often much faster than dissipation.

This simulation is carried out in TENS0 by defining the laser parameters and a function `laser_field_hadamard(t)` which returns the value of  $-\mu_0 E(t)$  with a maximum value of 3133.625  $\text{cm}^{-1}$ . The parameters for the bath are the same as those for the previous example outlined in Table 1 and the BCF portion of the input file requires no changes. The propagator must be modified to specify the time-dependent function and its associated operator,  $\sigma_x$ . The necessary changes to the previous example code are shown in Listing 3

```

1 # Final laser field parameters after unit
  conversions
2 t0_fs = 6.0
3 omega_rad_fs = 0.2825477
4 # The dipole has been incorporated into
  this value
5 interaction_max_cm = 3133.625
6 sigma_fs = 2.1233045
7 # Laser field function

```

```

8 def laser_field_hadamard(t):
9     #Returns the laser field interaction
    energy at time t (fs)
10    envelope = np.exp(-0.5 * ((t - t0_fs)
    / sigma_fs)**2)
11    # Unitless argument inside cos: (rad/
    fs) * fs = radians
12    carrier = np.cos(omega_rad_fs * t)
13    return -interaction_max_cm * envelope
    * carrier
14
15 end_time = 40.0 # fs
16 dt = 0.05 # fs
17 wfn = np.array([0.0, 1.0], dtype=np.
    complex128) # Start in Ground State
    |0> (convention [exc, gnd])
18 out = 'laser_example'
19 propagator = system_multibath(
20     fname='out',
21     init_rdo=np.outer(wfn, wfn.conj()),
22     # System Hamiltonian
23     sys_ham=np.array([[750, 0.0], [0.0,
    -750]]),
24     dtype=np.complex128),
25     # System-Bath coupling operator (
    Sigma_z / 2)
26     sys_ops=[np.array([[0.5, 0.0], [0.0,
    -0.5]]),
27     dtype=np.complex128)],
28     bath_correlations=[bath_simulation],
29     # Time-dependent driving function &
    Operator
30     td_f=laser_field_hadamard,
31     td_op=np.array([[0.0, 1.0], [1.0,
    0.0]]),
32     dtype=np.complex128), #(
    sigma_x)
33     dim=30,
34     end_time=end_time,
35     step_time=dt,
36 )

```

Listing 3: **Time-Dependent Hamiltonians:** Code for time-dependent simulations. Here, the time-dependent drive is defined as a python function and the parameters `td_f` and `td_op` are passed to the `system_multibath` propagator.

In Fig. 3 the system's state is driven to a superposition, however this half rotation in the Bloch sphere is not complete. The system state never reaches  $\frac{1}{\sqrt{2}}(|0\rangle + |1\rangle)$  and the coherences decay quickly due to dephasing, meaning that a noisy Hadamard gate has been modeled. This demonstrates TENS0's capability to simulate the impact of structured environmental noise on

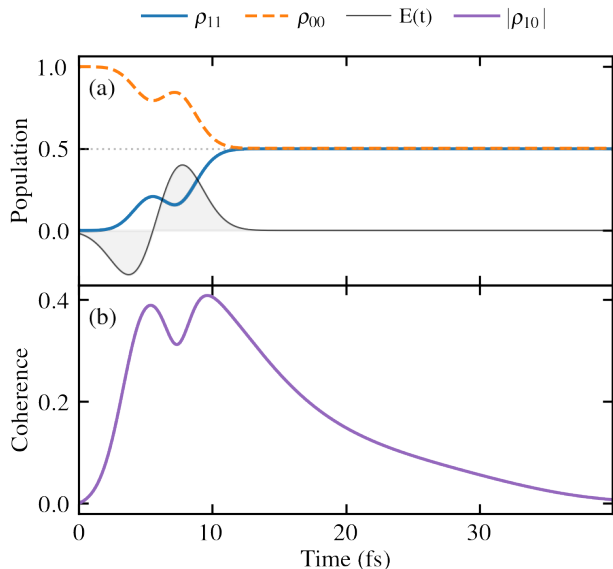


Figure 3: **Driven Spin-Boson Dynamics:** (a) Time evolution of populations and (b) coherence evolution under a resonant  $\pi/2$  Gaussian pulse while interacting with a structured bath. (c) The structured spectral density of the thermal bath. The laser-induced control dynamics demonstrates coherent excitation in the two-level system.

driven quantum systems, a situation relevant to many quantum control and quantum computing problems.

### 3.3.5 Adaptability of the Framework to Other Equations of Motion

Although the principal application of TENS0 and the principal focus of this tutorial is HEOM, the tensor network framework underlying the program is easily adapted to other equations of motion with propagators in sum of products form. In particular, this is demonstrated by the implementation of thermofield strategy for MCTDH in TENS0.<sup>93</sup> The thermofield strategy allows the wavefunction-based MCTDH to simulate finite temperature dynamics by mapping them to zero temperature dynamics in an extended Hilbert space.<sup>39,94,95</sup>

Performing a MCTDH calculation requires discretizing the bath, and the situation in Figure 1 requires a large discretization and significant computational resources. For the pur-

poses of this demonstration, a system with a single Brownian spectral density which does not require as many computational resources to achieve MCTDH convergence has been selected to compare to HEOM. The required changes to the simulation code to perform MCTDH are demonstrated in Listing 4. The HEOM modules are replaced with MCTDH modules and `gen_bcf` is replaced by `gen_star_boson` to perform the MCTDH discretized bath decomposition. The overall changes required to perform the simulation are minimal, demonstrating the versatility of TENS0's implementation framework and usage. The HEOM comparison for this example is generated by adjusting Listing 1 so that the bath contains only the Brownian mode specified in Listing 4. MCTDH calculations and their efficiency in comparison to HEOM calculations in TENS0's tensor network approach are largely beyond the scope of this tutorial and interested readers may find an in depth discussion in Ref. 93.

Despite our focus on HEOM rather than MCTDH, we would be remiss not to offer a general word on convergence. The discretization of the bath in MCTDH inevitably leads to recurrence and inaccuracy after a finite propagation time, which can be mitigated by increasing `n_discretization` but can never be escaped entirely. In Fig. 4, the selected discretization is sufficient for 200 fs, but not for 300 fs.

```

1 from math import ceil
2 import numpy as np
3 from tqdm import tqdm
4 # Import MCTDH module rather than HEOM
   modules
5 from tenso.prototypes.mctdh import
   system_multibath
6 from tenso.prototypes.bath import
   gen_star_boson
7
8 out = "mctdh"
9 # Generate the type of bath
   discretization required for MCTDH
10 bath_simulation = gen_star_boson(
11     re_b=[200],
12     width_b=[10],
13     freq_b=[50],
14     temperature=300,
15     cutoff=200, # Maximum frequency in the
   bath discretization
16     n_discretization=50, # Number of modes

```

```

17         in the discretization
18         discretization_method='TEDOPA', #
19         Method of choosing discrete modes
20     )
21 end_time = 200
22 dt = 1
23 wfn = np.array([0.0, 1.0], dtype=np.
24               complex128) # Initial wavefunction
25 propagator = system_multibath(
26     fname=out,
27     init_wfn=wfn, # The propagator
28     requires an initial wavefunction,
29     not density matrix
30     sys_ham=np.array
31     ([[[-750.0,300.0],[300.0,750.0]],
32      dtype=np.complex128),
33     sys_ops=[np.array([[[-0.5,0.0],
34                       [0.0,0.5]], dtype=np.complex128)],
35     baths=[bath_simulation], # Note the
36     different name for the bath input
37     end_time=end_time,
38     dim=8, # Dimension of each mode in the
39     discretization
40     step_time=dt,)
41 progress_bar = tqdm(propagator,total=ceil
42 (end_time/dt))
43 for _t in progress_bar:
44     progress_bar.set_description(f'@{_t:
45     .2f} fs')

```

Listing 4: **MCTDH Versus HEOM**: Code for a MCTDH calculation with a Brownian spectral density to compare to HEOM.

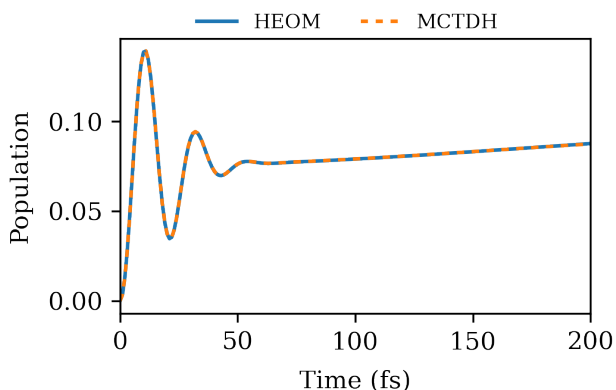


Figure 4: **MCTDH vs HEOM**. Short comparison of an MCTDH and HEOM calculation for a simple Brownian bath at 300 K and pure dephasing.

### 3.3.6 Convergence Parameters

TENSO has several parameters that control the numerical accuracy of the propagation including the time step size, propagation method, rank of the tensor network, hierarchy depth, and number of low temperature corrections included in the BCF decomposition. An increase in computational accuracy inevitably brings higher computational cost.

The simplest adjustment parameter is time step size. An initial step size which is too large may result in numerical problems or simulation failure. The initial step size is set by the parameter `step_time` in the propagator. A good rule of thumb is that it should be at most 1/20th of the fastest timescale in the problem.

The default propagation method in TENS0 begins with the use of an adaptive rank projection splitting method referred to in the code as `ps2`, which has a variable memory footprint, then transitions to a static rank, constant memory footprint direct integration method, `vmf`. This scheme should be appropriate for most uses. More information on adjusting the propagation method and error tolerances is located in section 5.4.

We will demonstrate convergence of calculations with respect to depth and rank using spin-boson models specified in Table 2. The first model in Fig. 5 (a) employs a symmetric model ( $\Delta\epsilon = 0$ ) with a purely DL bath, while (b) and (c) use an asymmetric system coupled to a combined DL and BO bath. The system Hamiltonian and system-bath coupling operator are the same as in Listing 1.

Truncation depth of the hierarchy expansion for each feature is controlled by the parameter `dim` in the propagator specifications. The default value is 5, but different models will require different depths. HEOM, when performed with an inadequate hierarchy depth, may produce dynamics with spurious oscillations or revivals<sup>30,96</sup> so it is crucial to check convergence with respect to hierarchy depth.<sup>65</sup> This issue is demonstrated in Fig. 5 (a), which performs the same calculations as in Listing 1 with a few modifications to the parameters. Only the DL term is used in the spectral density,

$\Delta\epsilon = 0$ , and the system-bath coupling operator is  $H_S = \sigma_x \otimes X_B$ . The truncation depth is set to  $\text{dim}=\mathbf{n}$  for each of  $n = 2, 4, 6, 10, 14, 25$ . Oscillations in the population when  $n$  is less than 25, whether very dramatic at  $n = 2$  or minimal at  $n = 14$ , are the result of insufficient hierarchy depth, but superficially resemble coherent dynamics that may occur in other quantum systems. Similar spurious oscillations can occur when insufficient low temperature corrections are included,<sup>65</sup> but this situation may produce not only spurious oscillations but physically unreasonable dynamics such as negative populations.<sup>97,98</sup> The number of low temperature correction terms included during the bath decomposition is determined by `n_ltc` during BCF construction. The default parameter is 0. The number required depends on the specific system and bath energy scales. For example, in Listing 1, `n_ltc=1` is sufficient. Note that the HEOM requires increasingly more features in the environment as the temperature is lowered and can become numerically intractable.

The tensor network rank is also a critical convergence parameter governing the accuracy of the simulations. Figs. 5 (b) and (c) display the convergence of the population dynamics with respect to the bond rank for the BTT and TT decompositions, respectively, in a case where  $H_{SB} = \sigma_z \otimes X_B$ . The simulations use the fixed rank `ps1` as the propagation strategy. The BTT structure in (b) exhibits quick convergence towards the reference solution (Rank = 40), whereas the TT decomposition in (c) requires significantly higher ranks to achieve comparable accuracy and displays unphysical artifacts at low ranks. The time-averaged absolute error versus the reference simulation,  $\langle |\Delta\rho_{11}| \rangle_t = \frac{1}{N_{\text{ts}}} \sum_{k=1}^{N_{\text{ts}}} |\rho_{11}(t_k) - \rho_{11}^{\text{ref}}(t_k)|$ , where  $N_{\text{ts}}$  is the number of time steps in the simulation, is shown in Fig. 5 (d) as a function of the parameter value for all three cases, providing a quantitative measure of convergence. The BTT rank converges most rapidly, reaching errors below  $10^{-3}$  at moderate rank values, while the TT decomposition and hierarchy depth require larger parameter values to achieve similar accuracy.

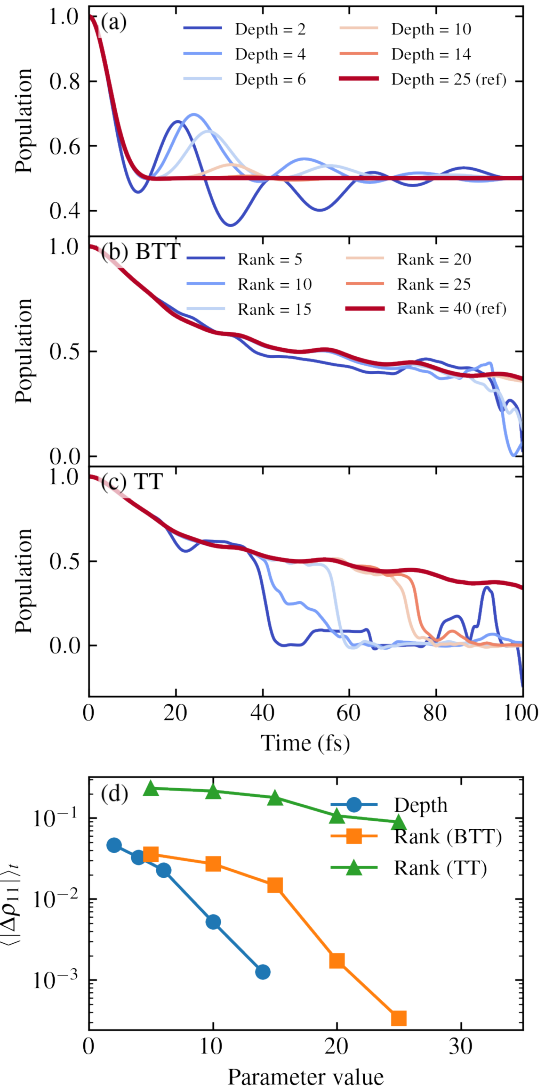


Figure 5: **Convergence Demonstration** (a) Population of a spin-boson model simulated with the BTT method for several different hierarchy depths demonstrating the spurious oscillations that occur when the depth is insufficient. (b) Population of a spin-boson model simulated with the BTT method for several different ranks showing less sensitivity to rank. (c) Population of a spin-boson model simulated with the TT method for several different ranks showing more sensitivity to rank. (d) Comparison of mean absolute deviation of population from reference population with depth and rank.

### 3.4 Example 2: FMO Complex With a Structured Environment

The Fenna–Matthews–Olson<sup>51,52</sup> complex is employed in studies of excitonic energy trans-

Table 2: Simulation parameters for the spin-boson models used in the convergence tests of Fig. 5. All parameters are given in  $\text{cm}^{-1}$ .

Parameter	Panel (a) ( $\text{cm}^{-1}$ )	Panel (b,c) ( $\text{cm}^{-1}$ )
$\Delta\epsilon$	0	1500
$V$	300	300
$\lambda, \omega_c$ (DL)	540, 70	540, 70
$\lambda, \eta, \omega'_0$ (BO)	0, 0, 0	330, 4, 1663

fer, coherence and entanglement in photosynthetic complexes, and for benchmarking new methods.<sup>57,99–102</sup> Studies have examined non-Markovian effects and the impact of different thermal baths on the FMO complex to improve our understanding of photosynthetic processes.<sup>53,55,103</sup> We will use the FMO complex to demonstrate TENS0’s utility in addressing larger systems with multiple baths and complicated descriptions of the environment spectral density involving three or more Brownian terms.

In the site basis, the FMO system Hamiltonian is

$$H_S = \sum_i \epsilon_i |i\rangle\langle i| + \sum_{i \neq j} V_{ij} (|i\rangle\langle j| + |j\rangle\langle i|), \quad (26)$$

where  $\epsilon_i$  denote site energies, and  $V_{ij}$  the couplings between sites  $i$  and  $j$ . The FMO complex is usually described by seven or eight sites, but we will use a reduced three site description to control computational cost. The three site model captures major features effectively<sup>104</sup> and will suffice for the purpose of our demonstration.

The matrix representation of the three site Hamiltonian in  $\text{cm}^{-1}$  is<sup>105</sup>

$$H_S = \begin{bmatrix} 200 & -87.7 & 5.5 \\ -87.7 & 320 & 30.8 \\ 5.5 & 30.8 & 0 \end{bmatrix}.$$

Most HEOM simulations of the FMO complex employ an independent bath with a Drude-Lorentz spectral density at each site. While this captures significant dynamical features, high-frequency modes—which substantially influence short-time behavior—are typically un-

derestimated;<sup>106</sup> thus simulations with more accurate spectral densities are desirable.<sup>107,108</sup> TENS0 makes studies incorporating structured spectral densities for this system computationally feasible for HEOM.

The system-bath coupling Hamiltonian is

$$H_{SB} = \sum_b \sum_i \hbar \omega_{b,i} \sqrt{2S_{b,i}} |i\rangle\langle i| \otimes X_B^{(b)}, \quad (27)$$

with  $S_{b,i}$  a Huang-Rhys factor and  $\omega_{b,i}$  the  $i$ th oscillator frequency of bath  $b$ . Note that each site is coupled to an independent bath. Our model approximates the spectral density via a sum of six underdamped Brownian oscillator terms which approximate one recently determined from spectroscopic measurements.<sup>109</sup>

Listing 5 contains the entire input file necessary to run the FMO example, excluding the import statements, which are identical to Listing 1. Note that a different propagation method is used in this simulation. Propagators are discussed more in section 5.4. We will make additional small modifications to this input file to compare the FMO dynamics with different thermal baths. First, we will run calculations at both 300 K and 77 K and use three low temperature corrections, `n_ltc=3`, for all 77 K calculations. Second, we will employ two simpler spectral densities, one using only the first three Brownian peaks, the three located below  $1000 \text{ cm}^{-1}$ , and one using a simple Drude-Lorentz spectral density with  $\lambda^{\text{DL}} = 35 \text{ cm}^{-1}$  and  $\omega_c^{\text{DL}} = 106.18 \text{ cm}^{-1}$ .<sup>105</sup> These three spectral densities are shown in Fig. 6 (c).

```

1 bath = gen_bcf(
2     re_b=[26.24, 13.832, 101.479, 57.575,
3         25.764, 9.126],
4     freq_b=[160, 247, 763, 1175, 1356,
5         1521],
6     width_b=[133, 53, 76, 29, 29, 15],
7     temperature=300,
8     decomposition_method='Pade',
9     n_ltc=1, # 3 needed at 77 K
10 )
11 h = np.array([
12     [200, -87.7, 5.5],
13     [-87.7, 320, 30.8],
14     [5.5, 30.8, 0]
15 ], dtype=np.complex128)

```

```

16 sys_ops = []
17 end_time = 1000.0
18 dt = 0.05
19 # Add a coupling operator for each site
20 for i in range(3):
21     op_i = np.zeros((3, 3))
22     op_i[i, i] = 1.0
23     sys_ops.append(op_i)
24
25 wfn = np.zeros(3)
26 wfn[0] = 1.0 # Initial state localized at
    site 1
27 out = "3_level_FMO_structured"
28 propagator = system_multibath(
29     fname=out,
30     init_rdo=np.outer(wfn, wfn.conj()),
31     sys_ham=h,
32     sys_ops=sys_ops,
33     # Couple an identical, independent
        bath to each site
34     bath_correlations=[bath, bath, bath],
35     end_time=end_time,
36     step_time=dt,
37     # Use a static rank projector
        splitting propagation method
38     ps_method="ps1",
39     dim=20,
40 )

```

Listing 5: **Three-site FMO quantum dynamics:** Input file for the simulation of the FMO complex. The ordering inside the `bath_correlations` list must match the ordering in the `sys_ops` list so that there is a one-to-one correspondance between system operators and baths.

In Fig. 6, we show the dynamics of the FMO complex under the six different baths. Population evolution with the simple Drude-Lorentz bath corresponds to dotted lines, solid lines correspond to the structured spectral density with all six Brownian peaks and the dashed lines denote the spectral density which uses only the three lowest frequency Brownian peaks. Significantly different population dynamics are observed for the three different spectral densities, with these differences being far more pronounced at lower temperature. Higher temperature suppresses population oscillations associated with coherent effects, an expected outcome.<sup>110</sup> The Drude-Lorentz spectral density produces very divergent dynamics in comparison to the more structured cases which, notably, have a higher total reorganization energy.

For the structured spectral density selected, apparent coherent oscillations are much less pronounced than for the Drude-Lorentz spectral density.

The employment of more realistic, structured spectral densities can have a large impact on the dynamics of the FMO complex. TENS0's ability to efficiently simulate systems with these features is a significant asset for treating photosynthetic complexes and related biological systems. The six Brownian peak spectral density at 77 K yields to  $K = 15$  features (12 from the BO features and 3 from the low temperature corrections) per site or 45 total features, which is significantly beyond the applicability of standard HEOM. Note that a thorough assessment of the appropriateness of this and other suggested structured spectral densities for the FMO complex is beyond the scope of this tutorial and this demonstration seeks only to emphasize their importance and TENS0's ability to address them.

### 3.5 Example 3: Entanglement Sudden Death

Entanglement between quantum subsystems plays a foundational role in quantum information science and other fields of modern physics.<sup>111–113</sup> Long-lived, controllable entanglement between subsystems is a key resource in quantum communication, quantum sensing, and quantum computing.<sup>113–116</sup> Entanglement has also become an important concept in quantum chemistry, offering new insights on electron correlations, molecular dynamics and open quantum systems.<sup>117–119</sup>

However, as a quantum system interacts with its environment, decoherence occurs and entanglement between subsystems decays, presenting a major challenge for hardware design in quantum technologies.<sup>86,87,120</sup> Density matrix coherence terms may decay exponentially depending on the interaction of an open quantum system with its environment but will remain finite at all times. Entanglement between subsystems, however, may decay to zero within finite time, a subject of intense research known as entanglement sudden death (ESD).<sup>59,121–126</sup>

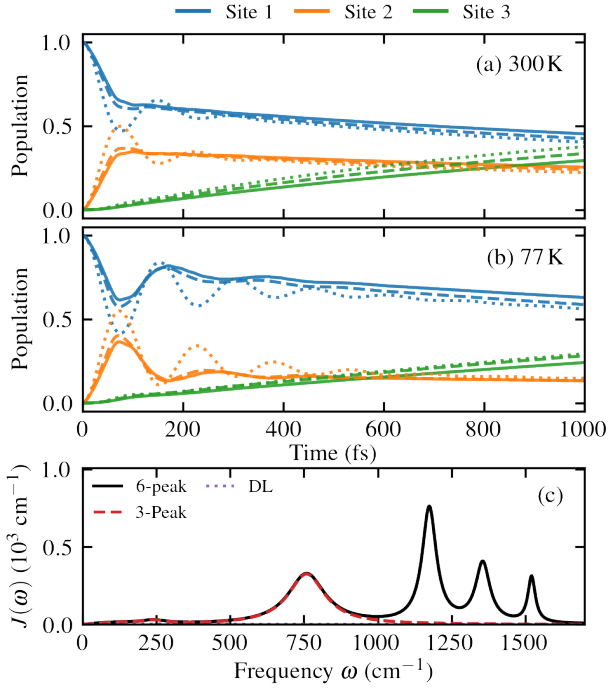


Figure 6: **Population Dynamics in the FMO Complex.** Population evolution at (a)  $T = 300$  K and (b)  $T = 77$  K for three sites, computed with the BTT tensor network decomposition for three different structured spectral densities (solid, dashed, and dotted lines). (c) The three structured spectral densities employed in the simulations.

The simplest system which can display meaningful entanglement is a pair of qubits, equivalently two spin-boson models. As the impact of bath models and non-Markovian effects are of keen interest in this simple model,<sup>127–131</sup> we use it as an example of the power of TENS0 to address problems in quantum information sciences.

We consider two qubits in an initially maximally entangled state,  $|\psi_0\rangle = \frac{1}{\sqrt{2}}(|01\rangle - |10\rangle)$ , each interacting with a local Bosonic bath. The system Hamiltonian is given by

$$H_S = \frac{\hbar\omega_1}{2}\sigma_z^{(1)} + \frac{\hbar\omega_2}{2}\sigma_z^{(2)} \quad (28)$$

where  $\sigma_z$  is the usual Pauli operator with the superscript indicating the qubit on which it operates and  $\omega_i$  are the frequencies of the qubits. The interaction between the system and baths

is given by

$$H_{SB} = \hbar\sigma_x^{(1)} \otimes X_B^{(1)} + \hbar\sigma_x^{(2)} \otimes X_B^{(2)}, \quad (29)$$

where the collective coordinates of each bath are distinguished by superscripts.

We measure entanglement using concurrence. Concurrence is defined for a two-qubit density matrix  $\rho$  using the spin-flipped state

$$\tilde{\rho} = (\sigma_y \otimes \sigma_y)\rho^*(\sigma_y \otimes \sigma_y) \quad (30)$$

where  $\rho^*$  is the complex conjugate of  $\rho$ . We compute the eigenvalues  $\lambda_1, \lambda_2, \lambda_3, \lambda_4$  of the matrix<sup>132</sup>

$$R = \sqrt{\sqrt{\rho}\tilde{\rho}\sqrt{\rho}} \quad (31)$$

and arrange them in decreasing order,  $\lambda_1 \geq \lambda_2 \geq \lambda_3 \geq \lambda_4$  then find the concurrence  $C(\rho)$  as

$$C(\rho) = \max(0, \lambda_1 - \lambda_2 - \lambda_3 - \lambda_4). \quad (32)$$

If  $C(\rho) > 0$  the state is entangled and if  $C(\rho) = 0$  the state is separable.

To simulate the pair of qubits, the Hamiltonian and bath parameters for the spin-boson problem demonstrated in Listing 1 are modified as shown in Listing 6. The initial state will be maximally entangled. We will make additional modifications to bath specifications of the Drude-Lorentz bath which, unless otherwise noted, has  $\lambda_{DL} = 50 \text{ cm}^{-1}$ ,  $\gamma_{DL} = 30 \text{ cm}^{-1}$ , and  $T = 300$  K.

```

1 # Define Pauli matrices
2 sigma_x = np.array([[0, 1], [1, 0]],
3                   dtype=np.complex128)
4 sigma_z = np.array([[1, 0], [0, -1]],
5                   dtype=np.complex128)
6 I = np.eye(2, dtype=np.complex128)
7 # Define parameters
8 omega = 20
9 # Define single qubit Hamiltonian
10 H1 = (omega / 2) * sigma_z + omega/2 * I
11 # Construct two-qubit Hamiltonian without
12 # interaction
13 h = np.kron(H1, I) + np.kron(I, H1)
14
15 Q_s1=np.kron(sigma_x,I)
16 Q_s2=np.kron(I,sigma_x)
17
18 sys_ops = [Q_s1,Q_s2] #The system
19 operators are sigma_x for both qubits

```

```

16
17 rdo_0 = np.array([[0, 0, 0, 0],
18                  [0, 0.5, -0.5, 0],
19                  [0, -0.5, 0.5, 0],
20                  [0, 0, 0, 0]],
21                  dtype=np.complex128) #This
                                     is the initial state
                                     of the two-qubit
                                     system
22
23 propagator = system_multibath(
24     fname=out,
25     init_rdo=rdo_0,
26     sys_ham=h,
27     sys_ops=sys_ops,
28     bath_correlations=[bath]*2,
29     end_time=end_time,
30     step_time=dt,
31     dim=45
32 )

```

Listing 6: **Entanglement Sudden Death:** Python code for concurrence time evolution of a two qubit system.

In Fig. 7, example population dynamics of the two qubits are displayed at 50 K where equilibration requires more than 150 fs to complete and populations are significantly biased in favor of the lower energy  $|00\rangle$  state. In Fig. 7 (b) and (c), we see that entanglement survival time increases with a lower temperature bath and smaller reorganization energy. Physically, larger  $\lambda$  indicates stronger system-bath coupling and environmental fluctuations, while a higher temperature  $T$  amplifies thermal noise, both of which strengthen decoherence channels that rapidly suppress entanglement.

For the sake of expediency, the bath was kept simple in this tutorial. The impact of varying even simple bath parameters is generally notable, and TENS0 allows for the systematic study of entanglement dynamics under more complicated, structured baths for more specialized applications in quantum information sciences.

## 4 TENS0 Structure

Having demonstrated applications of TENS0 in a variety of prototypical quantum dynamics problems, we now discuss those details of the implementation of TENS0 which are necessary

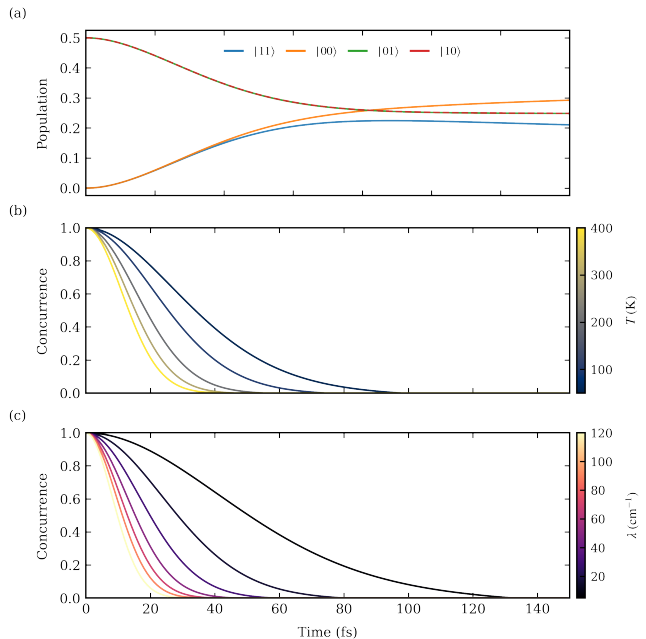


Figure 7: **Two-Qubit Quantum Dynamics and Entanglement Decay.** (a) Population dynamics of the two qubits at  $T = 50$  K. (b) Decay of the concurrence between the two qubits for varying temperature, with the color scale ranging from low (blue) to high (yellow) values. (c) Decay of the concurrence under variation of the reorganization energy  $\lambda$ , with the color scale ranging from weak (blue) to strong (magenta) system-bath coupling.

to understand in order to modify the framework or adjust functionality. The implementation of TENS0 contains four layers: (1) Interfaces with backend libraries. (2) Implementations of the general TTN decomposition for a time-dependent master equation with a generator in a sum-of-product (SoP) form. (3) Specific master equation implementations with TTN decompositions, currently including HEOM and MCTDH. (4) Functions which serve as templates to quickly specify bath and propagation parameters and run simulations of physical relevance. This is the only layer with which most users will need to interact. Some additional helper functions support multiple layers. The outline of the code structure is shown in Fig. 8. We will discuss the layers in order. Note that much of TENS0 takes an object oriented approach and some familiarity with object oriented programming is assumed in this section.

## 4.1 Interfaces with Backend Libraries

In `tenso.backend`, dependencies and global package settings for `pytorch`, `numpy`, and `torchdiffeq` are handled. This includes specifying `cpu` and `gpu` options for `pytorch` and importing or implementing integration methods. This file provides significant details on available integration methods other than the default adaptive time step Runge-Kutta.<sup>133</sup>

## 4.2 TTN Decomposition

The general master equations which **TENSO** is designed to address can be represented in the form  $\frac{d}{dt}\Omega(t) = \mathcal{L}(t)\Omega(t)$  where  $\Omega(t)$  is a high-dimensional tensor, and  $\mathcal{L}(t)$  is the generator of the dynamics. The implementation of the efficient propagation for general master equations is based on two components, the TTN representation of the  $\Omega(t)$  tensor and the SoP form of  $\mathcal{L}(t)$ .

In the `tenso.state` module, we implement the data structure for  $\Omega(t)$ . Specifically, `tenso.state.pureframe` defines the infrastructure needed to represent the underlying graph structure of the tensor network. The python class `Node` implements a node in the graph and each instantiated `Node` object is associated with a core tensor of the decomposition. The class `End` implements the open bonds in the tensor network. Both `Node` and `End` objects keep track of their neighbors through links, edges in the graph, and both are derived from the abstract `Point` class. A `Node` object may have more than one link, but an `End` object must have only one. The class `Frame` encodes the full graph of the topology of the tensor network. In `tenso.state.puremodel` we implement the tree tensor network vector  $\Omega(t)$  in the class `Model`. A `Model` object includes `Frame` object describing the TTN structure and data structures to associate a tensor valuation with every `Node` object in the `Frame`.

To specify the SoP generator of  $\mathcal{L}(t)$  we implement the class `SparseSPO` in `tenso.operator.sparse`. This class contains a list of dictionaries and each dictionary re-

presents an operator product in the sum. The keys are the names of degrees of freedom to operate on and the values are the corresponding local operators represented by matrices. We also implement the TDVP-based propagator class `SparsePropagator` in `tenso.operator.sparse`. This class generates the needed iterators for propagation with a given TTN vector of type `tenso.state.puremodel.Model` and a given SoP generator of type `tenso.operator.sparse.SparsePropagator`. Specific algorithms such as direct integration and projector-splitting (PS) algorithms<sup>14</sup> are implemented as methods in `SparsePropagator`.

## 4.3 Implementing Physical Master Equations as a TTN Master Equation

**TENSO** currently implements HEOM in `tenso.heom` and MCTDH, including the multilayer extension, in `tenso.mctdh`. In `tenso.heom.eom` we implement HEOM for a system coupled to one bath and in `tenso.heom.meom` we implement HEOM for a system coupled to multiple baths. Regardless of the master equation method, the class `Hierarchy` in the `meom` or `eom` module generates the needed data structure to construct a `tenso.operator.sparse.SparsePropagator`, as well as a `tenso.state.puremodel.Model`. The class `FrameFactory` implements construction of the TTN topologies for  $\Omega(t)$ , including the balanced tensor tree and tensor train topologies.

## 4.4 Templates for Common Problems

Interface templates for easy access to HEOM and MCTDH methods relevant to common physical problems are implemented in the subpackage `tenso.prototypes`. These functions hide all details of the calculation set up to facilitate ease of use. The `system_multibath` function employed in the examples is lo-

cated in `tenso.prototypes.heom`. This interface sets up the system state and propagator, including the tensor network topology requested. Similarly, the helper function `gen.bcf` employed to generate the composite spectral density is implemented in `tenso.prototypes.bath`. The default values of parameters are also found in this layer in `tenso.prototypes.default_parameters`.

## 4.5 Miscellaneous and Helper Functions

Additional capabilities are provided by helper functions. These include algorithms for traversing over a tree to visit all of the nodes and related tasks in `tenso.libs.utils`, and options to use a discrete variable representation (DVR) basis, rather than the default number basis, in the master equations, in `tenso.basis`. The most important of these auxiliary functions are those which handle the correlation function calculations necessary for computation. The correlation function object `Correlation` is found in `tenso.bath.correlation`. The necessary decomposition of the Bose-Einstein distribution is found in `tenso.bath.distribution` and `tenso.bath.sd` handles the definitions of different spectral densities.

## 5 Advanced Features

TENSO is an adaptable code. The preceding sections demonstrated its primary capabilities, features which are available without modification of any part of TENS0. This section outlines how to make simple modifications to the code to address specialized applications. We will demonstrate how to implement a custom topology for a TN, how to modify the metric to adjust the variant of HEOM, and detail some more advanced options for the functions shown in the examples.

### 5.1 Custom TN Implementation

TENS0 offers two predefined TN structures, the TT and  $n$ -ary BTT requested by set-

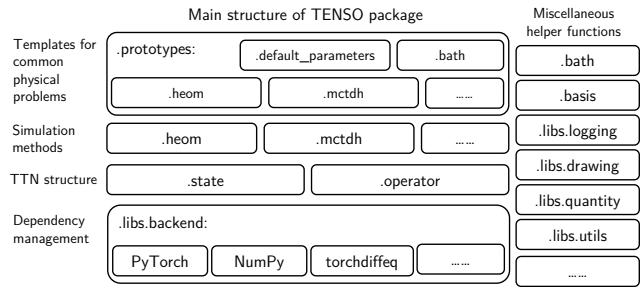


Figure 8: **Structure of TENS0.** The code TENS0 contains four main layers: (1) In `tenso.libs.backend` the needed data structures for handling a tensor array are imported from PyTorch and NumPy. (2) The tree tensor network (TTN) structure layer defines the data structures needed for a TTN state and the sum-of-product (SoP) operator, as well as the decomposed master equation and propagation schemes based on the TTN state and SoP dynamics generator. (3) In the simulation method layer, the physical master equations are specified in the TTN decomposition and the SoP dynamics generator. (4) The templates in the `prototypes` subpackage are interfaces to easily use specific master equation methods. TENS0’s structure allows users to access high-level functions to quickly perform calculations and allows developers easy access to low-level internal structures to build extensions and modifications.

ting `frame_method="train"` and `frame_method="treen"` respectively, (i.e. `frame_method="tree3"`). TENS0 supports arbitrary TTN structures specified by defining a root, a list of  $K$ -nodes, and the links between them. A new TTN structure is defined in the `FrameFactory` class of the file defining the relevant equation of motion, meaning either `MCTDH` or `HEOM` (`src/tenso/heom/meom.py` or `src/tenso/mctdh/eom.py` for HEOM and MCTDH respectively) using the methods `new_node()` and `add_link()`.

Listing 7 illustrates the implementation of a custom TT for a scenario with four total bath features in which the root node is placed in the center of the train rather than at either end. Once the frame “custom” is defined, the corresponding option must be registered in

the frame selection logic for `system_multibath` in `src/tenso/prototypes/heom.py` (or `src/tenso/prototypes/mctdh.py` for an MCTDH implementation) as shown in listing 8. The user can request the custom tree by passing `frame_method="custom"`, to `system_multibath`. The graphical representation of TENS0's default TT and the "custom" TT is shown in Fig. 9 where  $n_i$  for  $0 \leq i \leq 3$  are bath degrees of freedom and  $i$  and  $j$  are the system degrees of freedom.

```

1  # self refers to the FrameFactory
   instance
2  def custom(self) -> tuple[Frame, Node]:
3      k_max = self.bath_dof
4      frame = Frame()
5      # Instantiate nodes for the custom
       train
6      custom_train_nodes = [self._new_node()
   for _ in range(k_max + 2)]
7      root = custom_train_nodes[-1]
8
9      # Specifying the location of the
       leaves representing the system
       degrees of freedom
10     frame.add_link(root, self.sys_ket_end)
11     frame.add_link(root, self.sys_bra_end)
12     # Adding links between neighboring
       nodes
13     frame.add_link(custom_train_nodes[0],
   custom_train_nodes[1])
14     frame.add_link(custom_train_nodes[1],
   custom_train_nodes[2])
15     frame.add_link(custom_train_nodes[2],
   custom_train_nodes[3])
16     frame.add_link(custom_train_nodes[3],
   custom_train_nodes[4])
17     frame.add_link(custom_train_nodes[2],
   custom_train_nodes[-1])
18
19     # Specifying the location of the
       leaves representing bath degrees
       of freedom
20     frame.add_link(custom_train_nodes[0],
   self.chained_bath_ends[0])
21     frame.add_link(custom_train_nodes[1],
   self.chained_bath_ends[1])
22     frame.add_link(custom_train_nodes[3],
   self.chained_bath_ends[2])
23     frame.add_link(custom_train_nodes[4],
   self.chained_bath_ends[3])
24
25     return frame, root

```

Listing 7: **Custom TN Construction.** Python code defining a custom tensor network frame.

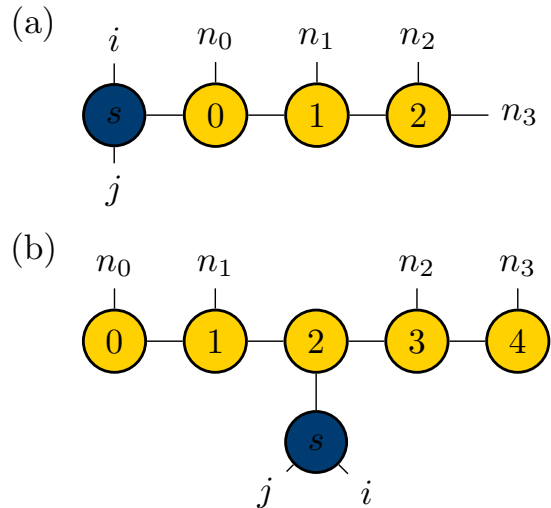


Figure 9: **TT Structures:** (a) Typical TT structure for a 4-feature bath. (b) Custom TT structure for a 4-feature bath. Nodes are represented by circles, system degrees of freedom are  $i$  and  $j$  and bath degrees of freedom are  $n_i$  for  $0 \leq i \leq 3$ .

```

1  # HEOM frame configuration:
2  frame_method = parameters['
   frame_method']
3  htd = FrameFactory(bath_correlation.
   k_max)
4
5  if frame_method.lower() == 'train':
6      frame, root = htd.train()
7  elif frame_method.lower().startswith('
   tree'):
8      n_ary = int(frame_method[4:])
9      frame, root = htd.tree(n_ary=n_ary
   )
10
11  elif frame_method.lower() == 'naive':
12      frame, root = htd.naive()
13  # Add these two lines
14  elif frame_method.lower() == 'custom':
15      frame, root = htd.custom()
16  else:
17      raise NotImplementedError(f'No
   frame_method {frame_method}.')

```

Listing 8: **Method Integration.** Python code for registering the custom method.

## 5.2 Custom BCF Implementation

The interface function `gen_bcf` handles the details of decomposing a BCF into the needed sum of exponentials form when its spectral density consists of DL and Brownian terms. It is possible to add custom spectral densities to `src/tenso/bath/sd.py`. In `TENSO`, a spectral density is a class which must extend the abstract `SpectralDensity` class. A custom spectral density class must implement a constructor, a function returning the spectral density at a given frequency  $\omega$ , and function returning a tuple containing lists of the residues and poles. Arguments accepting the new form of spectral density must be added to `src/tenso/prototypes/bath.py` in `gen_bcf` along with an option to initialize objects of the custom spectral density type and add them to the list of spectral densities used to generate the BCF.

A custom correlation function can be specified more easily if the complex coefficients,  $c_k$  and  $\gamma_k$  are known. The helper function `manual_corr_setup` in the `Correlation` class in `tenso.bath.correlation` performs this function. The process necessary to perform the manual initialization is shown in Listing 9. The `bath_simulation` produced can be passed to `system_multibath` as usual. Note that in `TENSO`  $c_k$  have units of energy squared and the  $\gamma_k$  have units of energy. For real  $\gamma_k$  only one feature will be introduced. For complex  $\gamma_k$ , the function will introduce a second feature with an exponent of  $\gamma_k^*$ . This may lead to redundant features when both  $\gamma_k$  and  $\gamma_k^*$  are needed to define  $C(t)$ .

```

1 from tenso.bath.correlation import
  Correlation
2 bath_simulation = Correlation() #
  Initialize an empty correlation object
3 # Replace contents of these lists with
  all the complex coefficients of the
  custom correlation function
4 c_coefficients = [c_1, c_2, c_3]
5 gamma_coefficients = [g_1, g_2, g_3]
6 # unit_convert=True indicates
  coefficients should be converted to
  internal TENSO units
7 bath_simulation.manual_corr_setup(

```

```

c_coefficients, gamma_coefficients,
unit_convert=True)

```

Listing 9: **Custom Correlation Function.** Code to initialize a custom correlation function.

## 5.3 Modifying the HEOM Variant

The metric for the operator of the  $k$ th bexciton or bath feature is  $\hat{z}_k|n_k\rangle = z_{k,n_k}|n_k\rangle$ , where  $|n_k\rangle$  is the excitation of the  $k$ th bexciton,  $\hat{n}_k|n_k\rangle = n_k|n_k\rangle$ . The commutator  $[\hat{z}_k, \hat{n}_k] = 0$  as these operators share a common eigenbasis. The dissipator  $\mathcal{D}_k$  in Eq. 14 associated with the  $k$ th bexciton exhibits a clear dependence on the metric. While every metric choice formally leads to identical physical results, different metrics correspond to distinct HEOM variants and specific choices may generate numerical instabilities. In `TENSO`, alternative HEOM variants may be realized by implementing a custom metric in the file defining the relevant equation of motion. A new metric for single-bath HEOM is defined in `src/tenso/heom/eom.py`, as shown in Listing 10. The custom metric is selected with the argument `metric='custom'` in the propagator.

```

1 @staticmethod
2 def _adm_factor(k: int, c: Correlation,
  metric: Literal['re', 'abs'] | complex
  = 're'):
3     c_k = c.coefficients[k]
4     cc_k = c.conj_coefficients[k]
5
6     if metric == 're':
7         f_k = np.sqrt(abs(c_k.real + cc_k.
  real) / 2.0)
8         if (c_k.imag + cc_k.imag) >
  EPSILON:
9             f_k *= -1.0
10    elif metric == 'abs':
11        f_k = np.sqrt((abs(c_k) + abs(cc_k
  )) / 2.0)
12    elif metric == 'custom':
13        # Define custom metric here
14        f_k = 1.0 # Placeholder
15    else:
16        f_k = complex(metric)
17
18    ... # Remainder of the function is not
  modified
19    return f_k

```

---

Listing 10:  
**Custom Metric Implementation.** Python code for defining the metric factor.

## 5.4 Propagation Scheme and Troubleshooting

There are several critical parameters governing the accuracy and efficiency of TENS0 propagation which were not reviewed in section 3.3.6. The primary parameter for adjustment of TENS0's propagation strategy is `stepwise_method` in `system_multibath` which determines the scheme for numerical propagation. By default, the `stepwise_method="mix"` method is selected. This approach represents a hybrid scheme, typically, combining a projector-splitting algorithm for the initial times followed by the direct integration method.<sup>14</sup> The other option is `stepwise_method="simple"` in which case only one propagation method is used for the entire simulation, selected by setting the argument `ps_method` equal to `"vmf"` for variable-mean field direct propagation, `"ps1"` for the static rank projector splitting method, and `"ps2"` for the adaptive rank projector splitting method.

When `"mix"` is selected, the initial phase of the propagation is controlled by the `system_multibath` parameters `auxiliary_ps_method` and `auxiliary_step_time`. The former specifies the propagation algorithm, which must be either `ps1` or `ps2`, while the latter defines the duration of this phase of propagation. The default is the adaptive rank `ps2` and the `max_auxiliary_rank` parameter sets the upper bound on the tensor rank. When the rank limit or the specified time threshold is reached, the propagation method changes to the method specified by the `ps_method` parameter, with `"vmf"` being the default.

The accuracy of the non-adaptive rank projector splitting algorithm, `ps1`, is determined by the tensor rank. In a mixed propagation beginning with `ps2` and transitioning to `ps1` or `vmf`, the second method will use the final rank selected by `ps2`. Otherwise, the value specified by the parameter `rank` is used. For the

rank-adaptive `ps2` propagator, accuracy and efficiency are determined by the maximum size of singular values (SVs) truncated during the algorithm. The argument `ps2_atol` defines the truncation threshold for singular values. To mitigate the loss of significant correlations during truncation, a fraction of discarded SVs are reincorporated, with this fraction determined by the `ps2_ratio`. The direct integration `vmf` method relies on standard ordinary differential equation solvers, with the method determined by the `ode_method` parameter. The default integration method is `dopri5`, a fifth order Runge-Kutta method, with additional options detailed in `tenso.libs.backend`. The error tolerances of the integrator are controlled by absolute, `ode_atol`, and relative, `ode_rtol`, tolerances.

The direct integration scheme also requires regularization of the equations of motion. The relevant parameters control the tolerance, `vmf_atol`, method `vmf_reg_method`, and procedure `vmf_reg_type`. Regularization is essential for the time evolution of the non-root tensors which require the inversion of a matrix that may be ill-conditioned. The `vmf_atol` parameter acts as a regularization term added to the diagonal elements of the ill-conditioned matrix to ensure invertibility. This regularization technique is always employed when the propagation scheme is set to `vmf`. Note that seriously ill-conditioned matrices are most likely to arise at the start of the simulation which is why the default mixed propagation scheme does not start with the `vmf` method.

The reliability and accuracy of TENS0's tensor network propagation strategies depends on interactions between control parameters. Depending on the system, one propagation method may be significantly more efficient or stable. In the case that a simulation is unsuccessful, it is possible that the problem is unsuitable for a tensor network compression, or it is possible that different control parameters are required for stable propagation. Decreasing the time step, changing between `vmf`, `ps1` or `ps2` propagation, or selecting an alternative integrator from `src/tenso/libs/backend` may improve the situation. Such cases should be carefully scrutinized for convergence.

## 5.5 Modifying Default Units

TENSO's default units are defined in `prototypes/default_parameters.py`. The units which TENS0 assumes when reading input from `system_multibath` and `bath_correlation` are defined in a dictionary, `default_units`, where keys are properties and values are strings corresponding to physical constants imported from SciPy, with the available list detailed in `libs/quantity.py`. Options for energy units include the default inverse centimeters, `"/cm"`, joules, `"J"`, electron volts, `"eV"`, and millielectron volts, `"meV"`. Options for time include the default femtoseconds, `"fs"`, seconds `"s"`, and picoseconds `"ps"`. Inverse temperature, not temperature, is defined, with the only option being the default, inverse Kelvin, `"/K"`.

TENS0 converts input into internal units and then scales energy and time by the factor associated with `"unital_energy"` in the `default_units` dictionary. Specifically any units of time or inverse temperature will be multiplied by this factor and any units of energy will be divided by this factor. The default value is 1000. Larger values may improve numerical performance when dealing with energies which are small in absolute terms. Similarly, smaller values may benefit performance for large absolute energies.

## 6 Conclusion

By combining the hierarchical equations of motion with tensor network representations TENS0 provides an efficient and systematically improvable framework that alleviates the curse of dimensionality inherent in conventional HEOM simulations. The resulting approach retains the formal exactness of HEOM while extending its applicability to complex spectral densities and arbitrary Hamiltonians, including those with explicit time dependence.

We demonstrated the versatility of TENS0 through a series of representative examples ranging from structured spin-boson models and driven two-level systems to the Fenna-Matthews-Olson complex to scenarios exhibiting entanglement sudden death. In each case,

TENS0 was able to capture rich dynamical behavior with reduced computational overhead, highlighting the efficiency of the TTN-based propagation scheme.

A key strength of TENS0 lies in its modular and extensible design. The package already incorporates GPU acceleration, multiple bath environments, and alternative correlation-function decompositions, providing both accessibility for non-specialists and flexibility for advanced users developing new approaches. It can easily be adapted to employ specialized and efficient correlation function decomposition schemes such as ESPRIT<sup>134–136</sup> and A4.<sup>137</sup> By exposing the underlying tensor operations and graph-based decomposition structures, TENS0 serves not only as a powerful simulation tool but also as a platform for further method development. Taken together, these features position TENS0 advantageously as a general and efficient framework for simulating quantum dynamics in complex environments.

## Data Availability

The data underlying this study are available in the published article and its Supporting Information.

**Acknowledgement** This material is based on work supported by the U.S. Department of Energy, Office of Science, Office of Basic Energy Sciences, Quantum Information Science Research in Chemical Sciences, Geosciences, and Biosciences Program under Award No. DE-SC0025334.

## References

- (1) Breuer, H.-P.; Petruccione, F. *The Theory of Open Quantum Systems*; Oxford University Press, 2007.
- (2) Nielsen, M. A.; Chuang, I. L. *Quantum Computation and Quantum Information*; Cambridge university press, 2010.
- (3) Weiss, U. *Quantum Dissipative Systems*; World Scientific, 2021.

- (4) Schlosshauer, M. *Decoherence and the Quantum-to-Classical Transition*; Springer, 2007.
- (5) Rivas, Á.; Huelga, S. F. *Open Quantum Systems: An Introduction*; Springer-Briefs in Physics; Springer: Berlin, Heidelberg, 2012.
- (6) Weimer, H.; Kshetrimayum, A.; Orús, R. Simulation methods for open quantum many-body systems. *Rev. Mod. Phys.* **2021**, *93*, 015008.
- (7) Xu, M.; Vadimov, V.; Stockburger, J. T.; Ankerhold, J. Colloquium: Simulating non-Markovian dynamics in open quantum systems. *Rev. Mod. Phys.* **2026**, –.
- (8) Zhan, Y.; Ding, Z.; Huhn, J.; Gray, J.; Preskill, J.; Chan, G. K.-L.; Lin, L. Rapid Quantum Ground State Preparation via Dissipative Dynamics. *Phys. Rev. X* **2026**, *16*, 011004.
- (9) Siddiqi, I. Engineering high-coherence superconducting qubits. *Nat. Rev. Mater.* **2021**, *6*, 875–891.
- (10) Gustin, I.; Kim, C. W.; McCamant, D. W.; Franco, I. Mapping electronic decoherence pathways in molecules. *Proc. Natl. Acad. Sci.* **2023**, *120*, e2309987120.
- (11) Kim, C. W.; Nichol, J. M.; Jordan, A. N.; Franco, I. Analog Quantum Simulation of the Dynamics of Open Quantum Systems with Quantum Dots and Microelectronic Circuits. *PRX Quantum* **2022**, *3*, 040308.
- (12) Kim, C. W.; Franco, I. General framework for quantifying dissipation pathways in open quantum systems. I. Theoretical formulation. *J. Chem. Phys.* **2024**, *160*.
- (13) Gustin, I.; Kim, C. W.; Franco, I. General framework for quantifying dissipation pathways in open quantum systems. III. Off-diagonal subsystem–bath couplings. *J. Chem. Phys.* **2026**, *164*, 034105.
- (14) Chen, X.; Franco, I. Tree tensor network hierarchical equations of motion based on time-dependent variational principle for efficient open quantum dynamics in structured thermal environments. *J. Chem. Phys.* **2025**, *163*.
- (15) Chen, X.; Franco, I. TENSOR. <https://github.com/ifgroup/pytenso>, 2025.
- (16) Tanimura, Y. Numerically “exact” approach to open quantum dynamics: The hierarchical equations of motion (HEOM). *J. Chem. Phys.* **2020**, *153*, 020901.
- (17) Chen, X.; Franco, I. Bexcitonics: Quasiparticle approach to open quantum dynamics. *J. Chem. Phys.* **2024**, *160*, 204116.
- (18) De Vega, I.; Alonso, D. Dynamics of non-Markovian open quantum systems. *Rev. Mod. Phys.* **2017**, *89*, 015001.
- (19) Nitzan, A. *Chemical Dynamics in Condensed Phases: Relaxation, Transfer, and Reactions in Condensed Molecular Systems*; Oxford Graduate Texts; OUP Oxford, 2024.
- (20) Mulvihill, E.; Geva, E. A Road Map to Various Pathways for Calculating the Memory Kernel of the Generalized Quantum Master Equation. *J. Phys. Chem. B* **2021**, *125*, 9834–9852.
- (21) Landi, G. T.; Kewming, M. J.; Mitchison, M. T.; Potts, P. P. Current fluctuations in open quantum systems: Bridging the gap between quantum continuous measurements and full counting statistics. *PRX Quantum* **2024**, *5*, 020201.
- (22) Anto-Sztrikacs, N.; Nazir, A.; Segal, D. Effective-Hamiltonian theory of open quantum systems at strong coupling. *PRX Quantum* **2023**, *4*, 020307.

- (23) Ikeda, T.; Scholes, G. D. Generalization of the hierarchical equations of motion theory for efficient calculations with arbitrary correlation functions. *J. Chem. Phys.* **2020**, *152*, 204101.
- (24) Ishizaki, A.; Tanimura, Y. Modeling vibrational dephasing and energy relaxation of intramolecular anharmonic modes for multidimensional infrared spectroscopies. *J. Chem. Phys.* **2006**, *125*.
- (25) Tanaka, M.; Tanimura, Y. Multistate electron transfer dynamics in the condensed phase: Exact calculations from the reduced hierarchy equations of motion approach. *J. Chem. Phys.* **2010**, *132*.
- (26) Bai, S.; Zhang, S.; Huang, C.; Shi, Q. Hierarchical equations of motion for quantum chemical dynamics: Recent methodology developments and applications. *Acc. Chem. Res.* **2024**, *57*, 3151–3160.
- (27) Kramer, T.; Noack, M.; Reinefeld, A.; Rodríguez, M.; Zelinsky, Y. Efficient calculation of open quantum system dynamics and time-resolved spectroscopy with distributed memory HEOM (DM-HEOM). *J. Comput. Chem.* **2018**, *39*, 1779–1794.
- (28) Seibt, J.; Kühn, O. Strong exciton–vibrational coupling in molecular assemblies. dynamics using the polaron transformation in HEOM space. *J. Phys. Chem. A* **2021**, *125*, 7052–7065.
- (29) Yan, Y.; Song, L.; Shi, Q. Understanding the free energy barrier and multiple timescale dynamics of charge separation in organic photovoltaic cells. *J. Chem. Phys.* **2018**, *148*.
- (30) Cainelli, M.; Tanimura, Y. Exciton transfer in organic photovoltaic cells: A role of local and nonlocal electron–phonon interactions in a donor domain. *J. Chem. Phys.* **2021**, *154*.
- (31) Yan, Y.; Liu, Y.; Xing, T.; Shi, Q. Theoretical study of excitation energy transfer and nonlinear spectroscopy of photosynthetic light-harvesting complexes using the nonperturbative reduced dynamics method. *Wiley Interdiscip. Rev. Comput. Mol. Sci.* **2021**, *11*, e1498.
- (32) Janković, V. Holstein polaron transport from numerically “exact” real-time quantum dynamics simulations. *J. Chem. Phys.* **2023**, *159*.
- (33) Lambert, N. et al. QuTiP 5: The Quantum Toolbox in Python. 2025; <http://arxiv.org/abs/2412.04705>, arXiv:2412.04705 [quant-ph].
- (34) Huang, Y.-T.; Kuo, P.-C.; Lambert, N.; Cirio, M.; Cross, S.; Yang, S.-L.; Nori, F.; Chen, Y.-N. An efficient Julia framework for hierarchical equations of motion in open quantum systems. *Commun. Phys.* **2023**, *6*, 313.
- (35) Kreisbeck, C.; Kramer, T. Long-Lived electronic coherence in dissipative exciton dynamics of light harvesting complexes. *J. Phys. Chem. Lett.* **2012**, *3*, 2828–2833.
- (36) Schollwöck, U. The density-matrix renormalization group in the age of matrix product states. *Ann. Phys.* **2011**, *326*, 96–192.
- (37) Wang, H.; Thoss, M. Multilayer formulation of the multiconfiguration time-dependent Hartree theory. *J. Chem. Phys.* **2003**, *119*, 1289–1299.
- (38) Lyu, N.; Soley, M. B.; Batista, V. S. Tensor-train split-operator KSL (TT-SOKSL) method for quantum dynamics simulations. *J. Chem. Theory Comput.* **2022**, *18*, 3327–3346.
- (39) Tamascelli, D.; Smirne, A.; Lim, J.; Huelga, S. F.; Plenio, M. B. Efficient simulation of finite-temperature open quantum systems. *Phys. Rev. Lett.* **2019**, *123*, 090402.

- (40) Bose, A.; Walters, P. L. A multisite decomposition of the tensor network path integrals. *J. Chem. Phys.* **2022**, *156*.
- (41) Cygorek, M.; Cosacchi, M.; Vagov, A.; Axt, V. M.; Lovett, B. W.; Keeling, J.; Gauger, E. M. Simulation of open quantum systems by automated compression of arbitrary environments. *Nat. Phys.* **2022**, *18*, 662–668.
- (42) Kundu, S.; Makri, N. PathSum: A C++ and Fortran suite of fully quantum mechanical real-time path integral methods for (multi-) system+ bath dynamics. *J. Chem. Phys.* **2023**, *158*.
- (43) Strathearn, A.; Kirton, P.; Kilda, D.; Keeling, J.; Lovett, B. W. Efficient non-Markovian quantum dynamics using time-evolving matrix product operators. *Nat. Commun.* **2018**, *9*, 3322.
- (44) Meyer, H.-D.; Manthe, U.; Cederbaum, L. The multi-configurational time-dependent Hartree approach. *Chem. Phys. Lett.* **1990**, *165*, 73–78.
- (45) Lindoy, L. P.; Rodrigo-Albert, D.; Rath, Y.; Rungger, I. pyTTN: An Open Source Toolbox for Open and Closed System Quantum Dynamics Simulations Using Tree Tensor Networks. 2025; <https://arxiv.org/abs/2503.15460>.
- (46) Raab, A. On the Dirac–Frenkel/Mclachlan variational principle. *Chem. Phys. Lett.* **2000**, *319*, 674–678.
- (47) Murnaghan, F. *J. Frenkel, Wave Mechanics; Advanced General Theory*; Clarendon Press, 1935.
- (48) Dirac, P. A. Note on exchange phenomena in the Thomas atom. Mathematical proceedings of the Cambridge philosophical society. 1930; pp 376–385.
- (49) Leggett, A. J.; Chakravarty, S.; Dorsey, A. T.; Fisher, M. P. A.; Garg, A.; Zwirger, W. Dynamics of the dissipative two-state system. *Rev. Mod. Phys.* **1987**, *59*, 1–85.
- (50) Mukamel, S. *Principles of Nonlinear Optical Spectroscopy*; Oxford University Press, USA, 1995.
- (51) Fenna, R.; Matthews, B. Chlorophyll arrangement in a bacteriochlorophyll protein from *Chlorobium limicola*. *Nature* **1975**, *258*, 573–577.
- (52) Matthews, B.; Fenna, R.; Bolognesi, M.; Schmid, M.; Olson, J. Structure of a bacteriochlorophyll a-protein from the green photosynthetic bacterium *Prosthecochloris aestuarii*. *J. Mol. Biol.* **1979**, *131*, 259–285.
- (53) Chenu, A.; Scholes, G. D. Coherence in energy transfer and photosynthesis. *Annu. Rev. Phys. Chem.* **2015**, *66*, 69–96.
- (54) Duan, H.-G.; Jha, A.; Chen, L.; Tiwari, V.; Cogdell, R. J.; Ashraf, K.; Prokhorenko, V. I.; Thorwart, M.; Miller, R. D. Quantum coherent energy transport in the Fenna–Matthews–Olson complex at low temperature. *Proc. Natl. Acad. Sci.* **2022**, *119*, e2212630119.
- (55) Hu, Z.; Liu, Z.; Sun, X. Effects of heterogeneous protein environment on excitation energy transfer dynamics in the Fenna–Matthews–Olson complex. *J. Phys. Chem. B* **2022**, *126*, 9271–9287.
- (56) Cao, J.; Cogdell, R. J.; Coker, D. F.; Duan, H.-G.; Hauer, J.; Kleinekathöfer, U.; Jansen, T. L.; Mančal, T.; Miller, R. D.; Ogilvie, J. P.; others Quantum biology revisited. *Sci. Adv.* **2020**, *6*, eaaz4888.
- (57) Jang, S. J.; Mennucci, B. Delocalized excitons in natural light-harvesting complexes. *Rev. Mod. Phys.* **2018**, *90*, 035003.
- (58) Gustin, I.; Kim, C. W.; Franco, I. Dissipation Pathways in a Photosynthetic Complex. *J. Phys. Chem. Letters* **2025**, *16*, 13093–13101.

- (59) Yu, T.; Eberly, J. H. Sudden death of entanglement. *Science* **2009**, *323*, 598–601.
- (60) Feynman, R.; Vernon, F. The theory of a general quantum system interacting with a linear dissipative system. *Ann. Phys.* **1963**, *24*, 118–173.
- (61) Caldeira, A. O.; Leggett, A. J. Path integral approach to quantum Brownian motion. *Phys. A: Stat. Mech. Appl.* **1983**, *121*, 587–616.
- (62) Suárez, A.; Silbey, R. Properties of a macroscopic system as a thermal bath. *J. Chem. Phys.* **1991**, *95*, 9115–9121.
- (63) Makri, N. The Linear Response Approximation and Its Lowest Order Corrections: An Influence Functional Approach. *J. Phys. Chem. B* **1999**, *103*, 2823–2829.
- (64) Hu, J.; Xu, R.-X.; Yan, Y. Communication: Padé spectrum decomposition of Fermi function and Bose function. *J. Chem. Phys.* **2010**, *133*.
- (65) Ishizaki, A.; Tanimura, Y. Quantum dynamics of system strongly coupled to low-temperature colored noise bath: Reduced hierarchy equations approach. *J. Phys. Soc. Jpn.* **2005**, *74*, 3131–3134.
- (66) Tanimura, Y.; Kubo, R. Time Evolution of a Quantum System in Contact with a Nearly Gaussian-Markoffian Noise Bath. *J. Phys. Soc. Jpn.* **1989**, *58*, 101–114.
- (67) Ke, Y. Tree tensor network state approach for solving hierarchical equations of motion. *J. Chem. Phys.* **2023**, *158*, 211102.
- (68) Ke, Y.; Borrelli, R.; Thoss, M. Hierarchical equations of motion approach to hybrid Fermionic and Bosonic environments: Matrix product state formulation in twin space. *J. Chem. Phys.* **2022**, *156*.
- (69) Yan, Y.; Xu, M.; Li, T.; Shi, Q. Efficient propagation of the hierarchical equations of motion using the Tucker and hierarchical Tucker tensors. *J. Chem. Phys.* **2021**, *154*.
- (70) Eckart, C.; Young, G. The approximation of one matrix by another of lower rank. *Psychometrika* **1936**, *1*, 211–218.
- (71) Grasedyck, L. Hierarchical singular value decomposition of tensors. *SIAM J. Matrix Anal. Appl.* **2010**, *31*, 2029–2054.
- (72) Grasedyck, L.; Hackbusch, W. An introduction to hierarchical (H-) rank and TT-rank of tensors with examples. *Comput. Methods Appl. Math.* **2011**, *11*, 291–304.
- (73) Harris, C. R.; Millman, K. J.; Van Der Walt, S. J.; Gommers, R.; Virtanen, P.; Cournapeau, D.; Wieser, E.; Taylor, J.; Berg, S.; Smith, N. J.; others Array programming with NumPy. *Nature* **2020**, *585*, 357–362.
- (74) Virtanen, P. et al. SciPy 1.0: Fundamental Algorithms for Scientific Computing in Python. *Nat. Methods* **2020**, *17*, 261–272.
- (75) Ansel, J.; Yang, E.; He, H.; Gimelshein, N.; Jain, A.; Voznesensky, M.; Bao, B.; Bell, P.; Berard, D.; Burovski, E.; others Pytorch 2: Faster machine learning through dynamic python bytecode transformation and graph compilation. Proceedings of the 29th ACM International Conference on Architectural Support for Programming Languages and Operating Systems, Volume 2. 2024; pp 929–947.
- (76) Chen, R. T. Q. torchdiffeq. <https://github.com/rtqichen/torchdiffeq>, 2018.
- (77) da Costa-Luis, C. et al. tqdm: A fast, Extensible Progress Bar for Python and CLI. <https://doi.org/10.5281/zenodo.14231923>, 2024.

- (78) Hunter, J. D. Matplotlib: A 2D graphics environment. *Computing in Science & Engineering* **2007**, *9*, 90–95.
- (79) Kumar, P.; Athulya, K.; Ghosh, S. Equivalence between the second order steady state for the spin-boson model and its quantum mean force Gibbs state. *Phys. Rev. B* **2025**, *111*, 115423.
- (80) Suárez, G.; Lobejko, M.; Horodecki, M. Dynamics of the nonequilibrium spin-boson model: A benchmark of master equations and their validity. *Phys. Rev. A* **2024**, *110*, 042428.
- (81) Wenderoth, S.; Breuer, H.-P.; Thoss, M. Non-Markovian effects in the spin-boson model at zero temperature. *Phys. Rev. A* **2021**, *104*, 012213.
- (82) Nesi, F.; Paladino, E.; Thorwart, M.; Grifoni, M. Spin-boson dynamics beyond conventional perturbation theories. *Phys. Rev. B* **2007**, *76*, 155323.
- (83) Deng, T.; Yan, Y.; Chen, L.; Zhao, Y. Dynamics of the two-spin spin-boson model with a common bath. *J. Chem. Phys.* **2016**, *144*.
- (84) Sun, K.; Kang, M.; Nuomin, H.; Schwartz, G.; Beratan, D. N.; Brown, K. R.; Kim, J. Quantum simulation of spin-boson models with structured bath. *Nat. Commun.* **2025**, *16*, 4042.
- (85) Peropadre, B.; Zueco, D.; Porras, D.; García-Ripoll, J. J. Nonequilibrium and nonperturbative dynamics of ultrastrong coupling in open lines. *Phys. Rev. Lett.* **2013**, *111*, 243602.
- (86) Kjaergaard, M.; Schwartz, M. E.; Braumüller, J.; Krantz, P.; Wang, J. I.-J.; Gustavsson, S.; Oliver, W. D. Superconducting qubits: Current state of play. *Annu. Rev. Condens. Matter Phys.* **2020**, *11*, 369–395.
- (87) Chirulli, L.; Burkard, G. Decoherence in solid-state qubits. *Adv. Phys.* **2008**, *57*, 225–285.
- (88) Garwola, J.; Segal, D. Open quantum systems with noncommuting coupling operators: An analytic approach. *Phys. Rev. B* **2024**, *110*, 174304.
- (89) Palm, T.; Nalbach, P. Suppressing relaxation through dephasing. *Phys. Rev. A* **2021**, *103*, 022206.
- (90) Gribben, D.; Rouse, D. M.; Iles-Smith, J.; Strathearn, A.; Maguire, H.; Kirton, P.; Nazir, A.; Gauger, E. M.; Lovett, B. W. Exact dynamics of non-additive environments in non-Markovian open quantum systems. *PRX Quantum* **2022**, *3*, 010321.
- (91) Palm, T.; Nalbach, P. Quasi-adiabatic path integral approach for quantum systems under the influence of multiple non-commuting fluctuations. *J. Chem. Phys.* **2018**, *149*.
- (92) McCall, S. L.; Hahn, E. L. Self-induced transparency by pulsed coherent light. *Phys. Rev. Lett.* **1967**, *18*, 908.
- (93) Chen, X.; Franco, I. Comparison between explicit and implicit discretization strategies for a dissipative thermal environment. *J. Chem. Phys.* **2026**, *164*.
- (94) Takahashi, Y.; Umezawa, H. Thermo field dynamics. *Int. J. Mod. Phys. B* **1996**, *10*, 1755–1805.
- (95) Takahashi, H.; Borrelli, R. Discretization of structured bosonic environments at finite temperature by interpolative decomposition: Theory and application. *J. Chem. Theory Comput.* **2025**, *21*, 2206–2218.
- (96) Krug, M.; Stockburger, J. On stability issues of the HEOM method. *The European Physical Journal Special Topics* **2023**, *232*, 3219–3226.

- (97) Dunn, I. S.; Tempelaar, R.; Reichman, D. R. Removing instabilities in the hierarchical equations of motion: Exact and approximate projection approaches. *J. Chem. Phys.* **2019**, *150*.
- (98) Fay, T. P. A simple improved low temperature correction for the hierarchical equations of motion. *J. Chem. Phys.* **2022**, *157*.
- (99) Milder, M. T.; Brüggemann, B.; van Grondelle, R.; Herek, J. L. Revisiting the optical properties of the FMO protein. *Photosynth. Res.* **2010**, *104*, 257–274.
- (100) González-Soria, B.; Delgado, F. Quantum Entanglement in Fenna–Matthews–Olson Photosynthetic Light–Harvesting complexes: A Short Review of Analysis Methods. *Journal of Physics: Conference Series*. 2020; p 012026.
- (101) Kell, A.; Khmelnskiy, A. Y.; Reinot, T.; Jankowiak, R. On uncorrelated intermonomer Förster energy transfer in Fenna–Matthews–Olson complexes. *J. R. Soc. Interface* **2019**, *16*, 20180882.
- (102) Bose, A.; Walters, P. L. Impact of spatial inhomogeneity on excitation energy transport in the Fenna–Matthews–Olson complex. *J. Phys. Chem. B* **2023**, *127*, 7663–7673.
- (103) Rodríguez, L. E. H.; Kananenka, A. A. Systematic study of the role of dissipative environment in regulating entanglement and exciton delocalization in the Fenna–Matthews–Olson complex. *Phys. Rev. E* **2025**, *111*, 014143.
- (104) Schulze, J.; Kuhn, O. Explicit correlated exciton-vibrational dynamics of the FMO complex. *J. Phys. Chem. B* **2015**, *119*, 6211–6216.
- (105) Ishizaki, A.; Fleming, G. R. Theoretical examination of quantum coherence in a photosynthetic system at physiological temperature. *Proc. Natl. Acad. Sci. USA* **2009**, *106*, 17255–17260.
- (106) Lorenzoni, N.; Lacroix, T.; Lim, J.; Tamascelli, D.; Huelga, S. F.; Plenio, M. B. Full microscopic simulations uncover persistent quantum effects in primary photosynthesis. *Sci. Adv.* **2025**, *11*, eady6751.
- (107) Kim, C. W.; Choi, B.; Rhee, Y. M. Excited state energy fluctuations in the Fenna–Matthews–Olson complex from molecular dynamics simulations with interpolated chromophore potentials. *Phys. Chem. Chem. Phys.* **2018**, *20*, 3310–3319.
- (108) Maity, S.; Kleinekathöfer, U. Recent progress in atomistic modeling of light-harvesting complexes: A mini review. *Photosynth. Res.* **2023**, *156*, 147–162.
- (109) Lorenzoni, N.; Cho, N.; Lim, J.; Tamascelli, D.; Huelga, S. F.; Plenio, M. B. Systematic Coarse Graining of Environments for the Nonperturbative Simulation of Open Quantum Systems. *Phys. Rev. Lett.* **2024**, *132*, 100403.
- (110) Duan, H.-G.; Prokhorenko, V. I.; Cogdell, R. J.; Ashraf, K.; Stevens, A. L.; Thorwart, M.; Miller, R. D. Nature does not rely on long-lived electronic quantum coherence for photosynthetic energy transfer. *Proc. Natl. Acad. Sci.* **2017**, *114*, 8493–8498.
- (111) Horodecki, R.; Horodecki, P.; Horodecki, M.; Horodecki, K. Quantum entanglement. *Rev. Mod. Phys.* **2009**, *81*, 865–942.
- (112) Orszag, M.; Hernandez, M. Coherence and entanglement in a two-qubit system. *Adv. Opt. Photonics* **2010**, *2*, 229–286.
- (113) Aolita, L.; De Melo, F.; Davidovich, L. Open-system dynamics of entanglement: A key issues review. *Rep. Prog. Phys.* **2015**, *78*, 042001.

- (114) Ursin, R.; Tiefenbacher, F.; Schmitt-Manderbach, T.; Weier, H.; Scheidl, T.; Lindenthal, M.; Blauensteiner, B.; Jennewein, T.; Perdigues, J.; Trojek, P.; others Entanglement-based quantum communication over 144 km. *Nat. Phys.* **2007**, *3*, 481–486.
- (115) Jozsa, R.; Linden, N. On the role of entanglement in quantum-computational speed-up. *Pro. R. Soc. A: Math. Phys. Eng. Sci.* **2003**, *459*, 2011–2032.
- (116) Guo, X.; Breum, C. R.; Borregaard, J.; Izumi, S.; Larsen, M. V.; Gehring, T.; Christandl, M.; Neergaard-Nielsen, J. S.; Andersen, U. L. Distributed quantum sensing in a continuous-variable entangled network. *Nat. Phys.* **2020**, *16*, 281–284.
- (117) Huang, Z.; Wang, H.; Kais, S. Entanglement and electron correlation in quantum chemistry calculations. *J. Mod. Opt.* **2006**, *53*, 2543–2558.
- (118) Hartmann, L.; Dür, W.; Briegel, H.-J. Steady-state entanglement in open and noisy quantum systems. *Phys. Rev. A* **2006**, *74*, 052304.
- (119) Boguslawski, K.; Tecmer, P. Orbital entanglement in quantum chemistry. *Int. J. Quantum Chem.* **2015**, *115*, 1289–1295.
- (120) Zhang, W.-M. Exact master equation and general non-Markovian dynamics in open quantum systems. *Euro. Phys. J.: Spec. Top.* **2019**, *227*, 1849–1867.
- (121) Yu, T.; Eberly, J. Finite-time disentanglement via spontaneous emission. *Phys. Rev. Lett.* **2004**, *93*, 140404.
- (122) Mazzola, L.; Maniscalco, S.; Piilo, J.; Suominen, K.-A.; Garraway, B. M. Sudden death and sudden birth of entanglement in common structured reservoirs. *Phys. Rev. A* **2009**, *79*, 042302.
- (123) Almeida, M. P.; de Melo, F.; Hor-Meyll, M.; Salles, A.; Walborn, S.; Ribeiro, P. S.; Davidovich, L. Environment-induced sudden death of entanglement. *science* **2007**, *316*, 579–582.
- (124) Roszak, K.; Horodecki, P.; Horodecki, R. Sudden death of effective entanglement. *Phys. Rev. A* **2010**, *81*, 042308.
- (125) Parez, G.; Witzczak-Krempa, W. The fate of entanglement. *Preprint at <https://doi.org/10.48550/arXiv>* **2024**, *2402*.
- (126) Nair, A. N.; Arun, R. Postponing entanglement sudden death by quantum interferences. *Phys. Scr.* **2024**, *99*, 025113.
- (127) Wang, F.; Hou, P.-Y.; Huang, Y.-Y.; Zhang, W.-G.; Ouyang, X.-L.; Wang, X.; Huang, X.-Z.; Zhang, H.-L.; He, L.; Chang, X.-Y.; others Observation of entanglement sudden death and rebirth by controlling a solid-state spin bath. *Phys. Rev. B* **2018**, *98*, 064306.
- (128) Ficek, Z.; Tanaś, R. Dark periods and revivals of entanglement in a two-qubit system. *Phys. Rev. A* **2006**, *74*, 024304.
- (129) Ma, J.; Sun, Z.; Wang, X.; Nori, F. Entanglement dynamics of two qubits in a common bath. *Phys. Rev. A* **2012**, *85*, 062323.
- (130) Jiang, W.; Wu, F.-Z.; Yang, G.-J. Non-Markovian entanglement dynamics of open quantum systems with continuous measurement feedback. *Phys. Rev. A* **2018**, *98*, 052134.
- (131) Bellomo, B.; Lo Franco, R.; Compagno, G. Entanglement dynamics of two independent qubits in environments with and without memory. *Phys. Rev. A* **2008**, *77*, 032342.
- (132) Wootters, W. K. Entanglement of formation and concurrence. *Quantum Inf. Comput.* **2001**, *1*, 27–44.
- (133) Dormand, J. R.; Prince, P. J. A family of embedded Runge-Kutta formulae. *J. Comput. Appl. Math.* **1980**, *6*, 19–26.

- (134) Roy III, R. H.; Kailath, T. ESPRIT–Estimation of signal parameters via rotational invariance techniques. *Opt. Eng.* **1990**, *29*, 296–313.
- (135) Potts, D.; Tasche, M. Parameter estimation for nonincreasing exponential sums by Prony-like methods. *Linear Algebra Appl.* **2013**, *439*, 1024–1039.
- (136) Takahashi, H.; Rudge, S.; Kaspar, C.; Thoss, M.; Borrelli, R. High accuracy exponential decomposition of bath correlation functions for arbitrary and structured spectral densities: Emerging methodologies and new approaches. *J. Chem. Phys.* **2024**, *160*.
- (137) Hunt, A. C.; Althorpe, S. C. Exploiting the path-integral radius of gyration in open quantum dynamics. *J. Chem. Phys.* **2026**, *164*.